ADDIS ABABA UNIVERSITY

ADDIS ABABA INSTITUTE OF TECHNOLOGY

AFRICAN RAILWAY CENTER OF EXCELLENCE

FATIGUE CRACK GROWTH ANALYSIS OF THE LIGHT RAIL VEHICLE BRAKING DISC UNDER DIFFERENT BRAKING CONDITIONS INCLUDING EMERGENCY BRAKING

A Thesis in Railway Engineering (Rolling Stock Engineering)

By

Daniel Liyew

Supervisor: Dr. Celestin Nkundineza

Co-advisor: Dr. Ing Demis Alemu

November, 2019

Addis Ababa, Ethiopia

A Thesis

Submitted to the African Railway Center of Excellence, in Partial Fulfillment of the Requirements for the Degree of Master of Science

The undersigned have examined the thesis entitled '**Fatigue Crack Growth Analysis of the Light Rail Vehicle Braking Disc Under Different Braking Conditions Including Emergency Braking**' presented by **Daniel Liyew**, a candidate for the degree of **Master of Science in Railway Engineering (Rolling Stock)** and hereby certify that it is worthy of acceptance.

Dr. Celestin Nkundineza		
Advisor	Signature	Date
Dr. Ing Demis Alemu		
Co-advisor	Signature	Date
Mr. Behailu Mamo		
Internal Examiner	Signature	Date
Mr. Hairedin Ismael		
External Examiner	Signature	Date
Dr. Abrham Gebre		
Chair person	Signature	Date

UNDERTAKING

I certify that research work titled "**Fatigue Crack Growth Analysis of the Light Rail Vehicle Braking Disc Under Different Braking Conditions Including Emergency Braking**" is my own work. The work has not been presented elsewhere for assessment. Where material has been used from other sources it has been properly acknowledged / referred.

Signature

Daniel Liyew

ABSTRACT

Railway brake discs are the safety-critical components usually designed for up to ten years of operation. To guarantee the safety, fracture mechanics method is usually applied to perform the prediction of fatigue crack growth. The main purpose of this study is to analyze the stresses and fatigue crack propagation of disc brake under different speeds and load of AA-LRT train services.

Mechanical and thermo-mechanical fatigue crack can often be found on the friction surface of brake discs used in railway vehicles after a period of usage due to exposure on heavy thermal and mechanical stress during braking and radial crack patterns that mostly occur. A brake disc crack exhibits different initiation and propagation behaviors with respect to different braking conditions. In this paper, the effect of braking energy on brake disc fatigue crack evolution is investigated by using a novel Extended Finite Element Method (XFEM) implemented in ABAQUS software for a train operating at acceptable and over speed at room temperature (25 ^{o}C) and at higher temperature (500 ^{o}C). Simulations at 4, 8, 12, 16 and 20mm crack length reveal that crack propagation the maximum effective stress intensity factor increase from as the crack length increased and accordingly the crack propagation rate increases at the crack size become large. On the other hand, the effect of temperature and speed were observed from the results to contribute to the increase of crack propagation for larger crack size.

In all cases, over speed and high temperature, as the braking is applied repeatedly, lead to increased propagation rate of the crack on the friction surface of the disc.

Keywords: *Brake disc, Mechanical stress, Thermal stress, Crack propagation*

ACKNOWLEDGMENTS

I want to convey my special thanks to my thesis advisor Dr. Celestin NKUNDINEZA for his support, guidance, inspiration and patience during my research study, I have greatly benefited from his knowledge and experience.

I would like to thank Dr. Ing. Demis Alemu for his encouragement and the importance of such research topic. Also, my sincere gratitude goes to Mr. Behailu Mamo (PhD candidate) for supplying me materials for laying the foundation of fracture mechanics science.

Lastly, I would like to thank all my friends and those who always gave me fruitful suggestions and shared their knowledge with me.

TABLE OF CONTENTS

ABSTRACT ..... **IV**

ACKNOWLEDGMENTS ..... **V**

TABLE OF CONTENTS ..... **VI**

LIST OF TABLES ..... **IX**

LIST OF FIGURES ..... **X**

ABBREVIATIONS ..... **XII**

CHAPTER 1 INTRODUCTION **1**

1.1 Background 1

1.1.1 Vehicle braking 2

1.1.2 Classification of brakes (based on transformation of energy) 3

1.2 Statements of the problem 6

1.3 Objectives of the study 7

1.3.1 General Objectives 7

1.3.2 Specific Objectives 7

1.4 Significance of the research 7

1.5 Scope and Limitation of the research 8

1.6 Organization of the Research (Thesis Structure) 8

1.7 Research methods 9

CHAPTER 2 LITERATURE REVIEW **11**

2.1 Introduction 11

2.2 Fracture Mechanics 12

2.3 Related Literature Reviews 13

CHAPTER 3 ANALYSIS AND MODELLING **18**

3.1 Thermo- Mechanical Analysis of rotor disc brake with Analytical Method 18

3.1.1 Main Technical Parameter 18

3.1.2 Thermal Transient Analysis of the Disc Brake 20

3.2 Numerical Model of Disc Brake 22

3.2.1 Analysis of Disc Rotor Force 23

3.2.2 Train Braking Energy at Level or Horizontal Track 24
3.2.3 Brake Force at Level or Horizontal Track 25
3.2.4 Heat Generated During Braking at Downhill Gradient 25
3.2.5 Braking Force of a Train on Downhill Motion at Train Downhill Position 26
3.3 Material Properties of Gray Cast Iron 27
3.4 Initial Temperature of Disc for the Next Braking 30
3.5 Determination of Locomotive Load Condition 31
3.5.1 Weight Transfer during Braking Condition 31
3.6 Physical Model of Disc Brake 32
3.7 Determination of the Friction Surface and Parameters of Disc and Pad 33
3.7.1 Determination of the Load on a Disc 33
3.7.2 Pressure determination for the brake caliper 33
3.7.3 Data for Train Acceptable Load Condition 34
3.7.4 Calculation of Effective Stress Intensity Factor 35
3.7.5 The Analysis of the Crack Propagation Life 36
3.8 XFEM Analysis in Abaqus 37
3.8.1 ABAQUS Software Package 37
3.8.2 Brake Disc Geometry Simplification 38
3.9 Elastic-Plastic Brake Disc Material Properties 39
3.9.1 Units in ABAQUS Analysis 40
3.9.2 Convergence Issue Handling 43
3.9.3 Geometrical Modeling of Disc and Pad Using Solid-work Software 44
3.9.4 Boundary Condition, Loads, and Constraints 45
3.9.5 Meshing of the Disc 46
CHAPTER 4 XFEM RESULT AND DISCUSION 47
4.1 XFEM ABAQUS Result 47
4.1.1 Effect of Mechanical (Static) Load 47

4.1.2 Combined Effect of Frictional Heating Temperature and Mechanical Load ……51
4.2 The Curve of the Maximum Principle Stress in Crack Length 60
4.3 The Curve of Stress Intensity Factor at Crack front Point 60
4.4 The Curve of Stress Intensity Factor in Crack Extension 64
4.5 Discussions 66
CHAPTER 5 CONCLUSION AND RECOMMENDATION 67
5.1 Conclusion 67
5.2 Recommendations and Future work 68
REFERENCES 69
APPENDIX 74

LIST OF TABLES

Table 3-1: Seating capacity of the train [21] 18
Table 3-2: Weights of the train [21] 18
Table 3-3: Type of brake and mounting place [21] 19
Table 3-4: Type of brake and way of application [21] 19
Table 3-5: Material properties of gray cast iron [27] 27
Table 3-6: Data for calculating heat flux 32
Table 3-7: Dimension of disc and brake pad for railway locomotives 33
Table 3-8: calculated and collected emergency brake data at 40 km/hr 34
Table 3-9: calculated and collected emergency brake data at 80 km/hr 34
Table 3-10: Common consistent units 41
Table 3-11: Elastic material behavior of the disc material [27][37] 41
Table 3-12: Plastic region behavior of the disc material at 25 ^{O}C [43] 42
Table 3-13: Plastic region behavior of the disc material at 500 ^{0}C[43] 42
Table 3-14: Temperature dependent thermal properties used in ABAQUS [46][47][44] 42
Table 4-1: Maximum crack tip principal stress versus crack length 56
Table 4-2: Crack front point effective stress intensity factor versus Crack front point at 4mm crack length 56
Table 4-3: Crack front point effective stress intensity factor versus Crack front point at 8mm crack length 56
Table 4-4: Crack front point effective stress intensity factor versus Crack front point at 12mm crack length 57
Table 4-5: Crack front point effective stress intensity factor versus crack front point at 16mm crack length 57
Table 4-6: Crack front point effective stress intensity factor versus Crack front point at 20mm crack length 58
Table 4-7: Effective stress intensity factor versus crack extension 59
Table 4-8: Crack propagation rate (da/dN) versus crack length 59
Table 4-9: Number of failure cycle versus crack length 59

LIST OF FIGURES

Figure 1-1: Richard Trevithick's engine from 1804 a), the world speed recorder TGV from 2007 b) [1].....2
Figure 1-2: Schematic Views of Drum and Disc Brakes [2].....3
Figure 1-3: wheel mounted disc brakes of unpowered bogie [4]. 4
Figure 1-4: axle mounted disc brakes of powered bogie [4]. 4
Figure 1-5: working principle of disc brake bolted to the wheel (a) [6] and fitted (mounted) to the axle (b) [7].....5
Figure 1-6: Procedure of research.....10
Figure 2-1**:** The three loadings of crack: (a) Tension (b) Shear (c) Tearing [12].....12
Figure 3-1: Three-dimensional heat conduction through a disc volume element 21
Figure 3-2: Free body diagram of wheel rotor system 23
Figure 3-3: velocity vs. time graph.....30
Figure 3-4: Meshing of Disc in ANSYS.....34
Figure 3-6: Emergency braking in downhill and recommended load condition 35
Figure 3-7: The schematic picture of the SEB on a thermal fatigue cracked brake disc..35
Figure 3-8: The disc region to be simplified Figure 3-9: Simplified wheel geometry...38
Figure 3-10: A typical stress-strain curve [40].....39
Figure 3-11: (a) 3D model of Disc (b) 3D model of Pad.....44
Figure 3-12: Disc and Pad assembling model 45
Figure 3-13:(a) Boundary Conditions and Loads, (b) crack geometry.....45
Figure 3-14 Mesh details 46
Figure 4-1: Maximum principle stress in Mpa for 4mm crack length.....48
Figure 4-2: Maximum principle stress in Mpa for 8mm crack length.....48
Figure 4-3: Maximum principle stress in Mpa for 12mm crack length.....48
Figure 4-4: Maximum principle stress in Mpa for 16mm crack length.....49
Figure 4-5: Maximum principle stress in Mpa for 20mm crack length.....49
Figure 4-6: Maximum principle stress in Mpa for 4mm crack length.....50
Figure 4-7: Maximum principle stress in Mpa for 8mm crack length.....50
Figure 4-8: Maximum principle stress in Mpa for 12mm crack length.....50
Figure 4-9: Maximum principle stress in Mpa for 16mm crack length.....51
Figure 4-10: Maximum principle stress in Mpa for 20mm crack length.....51

Figure 4-11: Maximum principle stress in Mpa for 4 mm crack length.....52
Figure 4-12: Maximum principle stress in Mpa for 8 mm crack length.....52
Figure 4-13: Maximum principle stress in Mpa for 12 mm crack length.....52
Figure 4-14: Maximum principle stress in Mpa for 16 mm crack length.....53
Figure 4-15: Maximum principle stress in Mpa for 20 mm crack length.....53
Figure 4-16: Maximum principle stress in Mpa for 4 mm crack length.....54
Figure 4-17: Maximum principle stress in Mpa for 8 mm crack length.....54
Figure 4-18: Maximum principle stress in Mpa for 12 mm crack length.....54
Figure 4-19: Maximum principle stress in Mpa for 16 mm crack length.....55
Figure 4-20: Maximum principle stress in Mpa for 20 mm crack length.....55
Figure 4-21: Crack tip maximum principal stress versus Crack length.....60
Figure 4-22: Stress intensity factor versus Crack front point at 4 mm crack length 61
Figure 4-23: Stress intensity factor versus Crack front point at 8 mm crack length 62
Figure 4-24: Stress intensity factor versus Crack front point at 12 mm crack length 62
Figure 4-25: Stress intensity factor versus Crack front point at 16 mm crack length 63
Figure 4-26: Stress intensity factor versus Crack front point at 20 mm crack length 63
Figure 4-27: Effective stress intensity factor versus Crack length 64
Figure 4-28: Crack propagation rate versus crack length.....65
Figure 4-29: Number of cycles to failure versus crack length.....65

ABBREVIATIONS

ETCS	**European Train Control System**
WSP	**Wheel Slide Protection**
AALRT	**Addis Ababa Light Rail Transit**
EFEM	**Extended Finite Element Method**
GFEM	**General Finite Element Method**
LEFM	**Linear Elastic Fracture Mechanics**
MAXPS	**Maximum Principle Stress**
GVW	**Gross Train Weight**
SEB	**Bending Single-edge**

CHAPTER 1 INTRODUCTION

1.1 Background

Transport is one of the key sectors that play crucial roles in achieving the goals of poverty eradication and sustainable development. The transport center is very much linked to developments in other sectors of the economy. The history of the locomotive-hauled trains began in the early19th century. These two centuries, and especially the recent years, saw dynamic advances in the different fields of railway engineering, (Figure 1). The main reason for this is the considerable development of air and road transportation as concurrent transportation forms.

Railway transportation is the safest transportation system and has the smallest energy and space demand, compared to its competitors. Thus it provides an economical solution in both freight and passenger transportation. For long distances (500-600 Km), very high speed trains (250-350 Km/h) are possible choice instead of aviation [1]. As archduke Johann of the Austro-Hungarian monarchy said:

"*Railways reflect the culture and economic conditions of a country. Dense train traffic is proof of a lively economy, fast and reliable traffic is the best testimonial in the eyes of foreigners for a country's level of culture.*"

/Archduke Johann 1825/

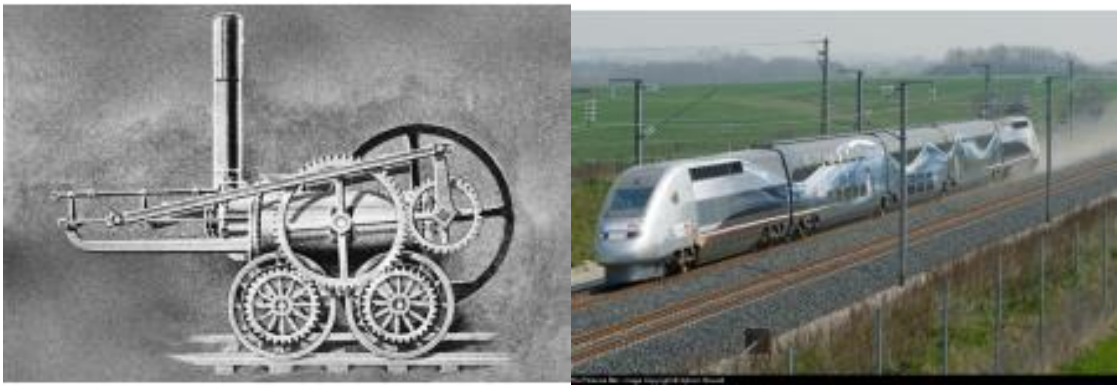

a) b)

Figure 1-1: Richard Trevithick's engine from 1804 a), the world speed recorder TGV from 2007 b) [1]

Development resulted in faster travelling speeds as well as better train safety systems. In addition to tread brake systems, disk brake and electromagnetic rail brake systems also appeared. Apart from the different new effective brake systems, automatic train control systems came into service as well (e.g. LZB in Germany, INDUSI in Austria, EVM in Hungary, ETCS in Europe, etc.) to minimize the risk of accidents on the rails all over the world. Further more like conventional road vehicles anti-skid devices, so called WSP systems (Wheel Slide Protection system), are applied also in railway vehicles[1].

Owing to these developments and others not mentioned above, rail transport has become one of the safest forms of transportation worldwide. However, these advances, beside their positive effects, also brought ever newer problems which researchers and experts had to solve.

For railway trains, the braking technology get fast pace worldwide, even the main brake method is electricity or eddy current brake but frictional brake is a redundancy backup and reliable way to stop the trains. Most form of frictional brakes on the railway locomotives is disc brake type mounted on wheels or axels to dissipate brake energy.

1.1.1 Vehicle braking

A brake is a device by means of which artificial frictional resistance is applied to moving train vehicle, in order to stop the motion of the train vehicle. In the process of performing this function, the brakes absorb either or both kinetic energy or potential energy of the moving vehicle. The energy absorbed by brakes is dissipated in the form of heat. This heat is dissipated in the surrounding atmosphere to stop the vehicle, so the brake system should have the following requirements:-

- The brakes must be strong enough to stop the vehicle within a minimum distance in an emergency.
- The driver must have proper control over the vehicle during braking and the vehicle must not skid.
- The brakes must have well anti fade characteristics i.e. their effectiveness should not decrease with constant prolonged application.
- The brakes should have well anti wear properties.

1.1.2 Classification of brakes (based on transformation of energy)

- Hydraulic brakes.
- Electric brakes.
- Mechanical brakes.

The mechanical brakes according to the direction of acting force are divided in to two groups.

Radial brakes:

In these brakes the force acting on the brake drum is in radial direction. The radial brake may be subdivided into external brakes and internal brakes. Example, Tread brake (brake shoe).

Axial brakes:

In these brakes the force acting on the brake drum is only in the axial direction. Example, Disc Brakes, Cone brakes etc. A more advanced form of the disc brake is the ventilated or vented disc, where internal cooling is achieved by air flowing through radial passages or vanes in the disc.

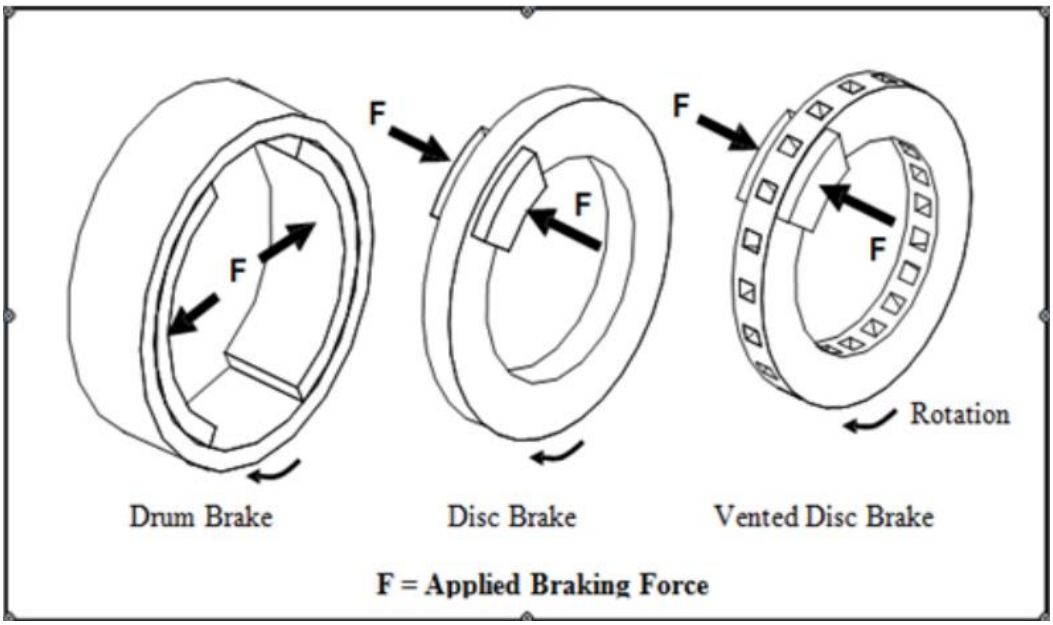

Figure 1-2: Schematic Views of Drum and Disc Brakes [2]

Disc brakes are widely used because it is simple, powerful, easy maintenance and allow new materials of disc and pad to be brought into use to provide effective friction and

minimize the wear. The premature wear and thermal cracking of brake discs are attributed to high thermal stress during brake process, more heat need to be distributed to disc rotor and brake pad friction pair, which cause higher thermal stress [3].

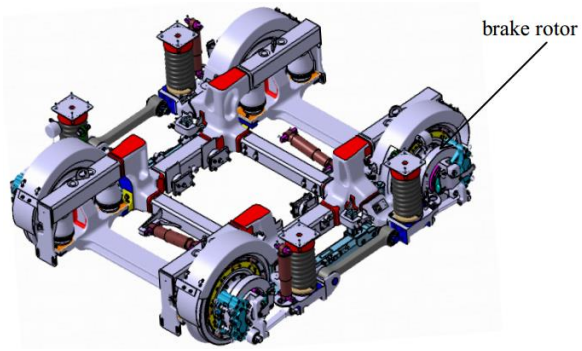

Figure 1-3: wheel mounted disc brakes of unpowered bogie [4].

The disc brake is a wheel brake which slows rotation of the wheel by the friction caused by pushing brake pads against a brake disc with a set of calipers. The disc brake is usually made of grey cast iron, structural steel, but may in some cases be made of composition such as reinforced carbon-carbon or ceramic matrix composition. This is associated to the Wheel or the axle. To stop the wheel, frictional material in the form of brake pads, mounted on a device called a brake caliper, is forced mechanically, hydraulically, pneumatically or electromagnetically against both sides of the disc. Friction causes the disc and attachment wheels pad to slowdown and Stop. Brakes convert motion to heat, and if the brakes get too hot, they become less effective and this phenomena is known as break fade [5].

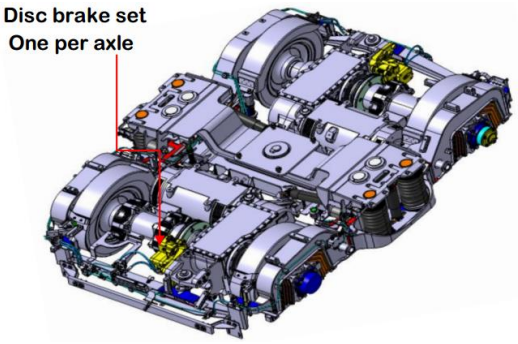

Figure 1-4: axle mounted disc brakes of powered bogie [4].

A disc brake consists of a cast iron disc bolted to the wheel hub or fitted (mounted) to the axle and a stationary housing called caliper. The caliper is connected to some stationary part of the vehicle, like the axle casing or the stub axle and is cast in two parts, each part

containing a piston. In between each piston and the disc, there is a friction pad held in position by retaining pins, spring plates etc. passages are drilled in the caliper for the fluid to enter or leave each housing. These passages are also connected to another one for bleeding. Each cylinder contains rubber-sealing ring between the cylinder and piston. A schematic diagram is shown in the figure.

Principle: the principle used is the applied force (pressure) acts on the brake pads, which comes into contact with the moving disc. At this point of time due to friction the relative motion is constrained.

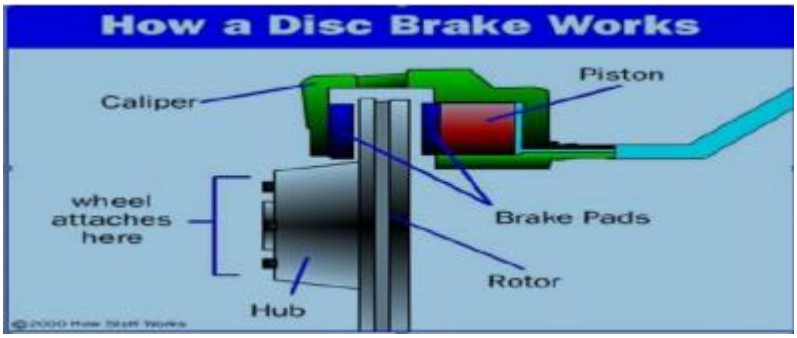

(a)

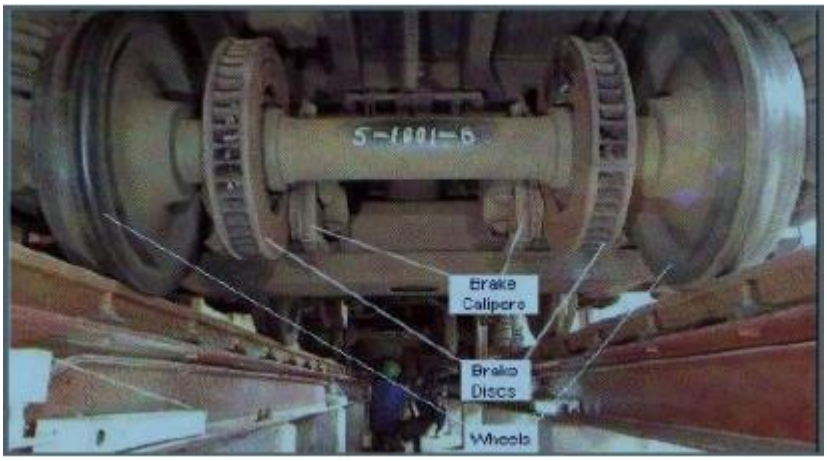

(b)

Figure 1-5: working principle of disc brake bolted to the wheel (a) [6] and fitted (mounted) to the axle (b) [7].

A number of researchers and studies has been made on the temperature field of train disc brake [8], investigation of temperature and thermal stress in Ventilated Disc Brake on 3D Thermo-Mechanical coupling model [9]. Researches on modelling thermal effect braking

of railway, using analytical and numerical modeling of thermal effect during long term braking for maintaining a constant speed on a down grade rail road by using finite element method (ANSYS) were done.

The cumulative results and findings of these studies and researches are focused thermal stress distribution and effect of temperature on disc brake and brake pad. The analysis of thermo-mechanical effect of disc brake problem during braking has been discovered enough and fatigue crack propagation at normal speed (40 km/hr) and over speed (80 km/hr) has not been studied in largely. Therefore, understanding of the fatigue crack propagation in disc brake which possibility of maximizing effectiveness and safety of the train and also used to determine number of failure cycle.

This study aims to understand fatigue crack propagation of brake disc and analyze the thermal, frictional and stress development phenomena during emergency braking at normal and over speed of contact occurs in brake pad and disc system, that to cause surface damage including crack to the disc surface during braking.

1.2 Statements of the problem

Disc overheating and rapid wear are the main problems that cause a decrease in braking performance. It also causes judder and noise which impose discomfort for the passengers and causes a stress on the rail. These all have a combined undesired effect that rise the lifecycle cost of the components. Thus, due to braking capacity limitation the speed of urban trains decreased significantly in order to stop the rail vehicle within a short distance possible safely while it has a smaller kinetic energy. Smaller speeds of urban trains result in poor customer satisfaction and can significantly reduce profit of railway companies. Increasing demand for faster trains with higher acceleration and deceleration demand high performance braking system is so important.

Over speeding during emergency braking may cause premature wear, bearing failure, and thermal cracks. Since the condition of braking is very much severe, then it is important to analyze the thermal and mechanical analysis of the disc brake with respect to over speeding and emergency braking.

Simulation of crack propagation effects was found to be most effective for crack growth and prediction of global disc behavior, with more sophisticated analysis required to

determine more detailed design limits. This paper will aim to investigate the fatigue crack growth of AALRT disc brake using Extended finite element (XFEM) analysis.

1.3 Objectives of the study

1.3.1 General Objectives

The focus of this study is to analyze the propagation behavior of surface initiated cracking on brake disc of AALRT trains using XFEM and investigation of thermal and structural deformation during a single braking cycle for maintaining a constant speed and braking to standstill afterwards on a downgrade rail tracks.

1.3.2 Specific Objectives

The specific objectives of this research are:

- Analyzing the thermal and mechanical behavior of the disc brake analytically.
- Analyzing the temperature distribution of the disc brake for both normal and over speed with emergency braking.
- Analyzing and simulate the deformations and stresses of the disc brake.
- Simulate the fatigue crack propagation on the disc at normal speed and at room temperature (25 ^{o}C) and at high temperature (500 ^{o}C) and aso at over speed and at room temperature (25 ^{o}C) and at high temperature (500 ^{o}C) on downhill train position by XFEM.
- Determining the number of failure cycles in disc at different crack extension.

1.4 Significance of the research

The Author strongly believes that this thesis has the following prominent values.

- The analysis steps and the modeling used in this paper are synergistically generated from different fields of science like Thermal and Fracture Mechanics sciences for railway application and have its own credit in idea generation in modeling fracture problems in relation to disc/pad contact phenomena.
- The finding of this research will serve as input to a more deep and advanced studies in the future.

- The finding and the steps are helpful for the safety periodic assessment and regulation need at glance for maintaining safe working cost for any railway companies.

1.5 Scope and Limitation of the research

Scope of the study focuses on

- Checking the degree of severity of railway brake disc in crack propagation.
- Estimating the frictional heat generated due to contact of disc and pad.
- Employment of Extended Finite Element (XFEM) based on the Cohesive segment approach for Elastic-Plastic (non-linear) material type and for Edge crack (surface crack) and Horizontal crack (Subsurface crack) at different initial length of the artificial cracks insertion on a simplified disc geometry using ABAQUS commercial software.

Limitation

Due to computational power required to model the interaction of brake pad and disc in dynamic state (could take several months with current computational power available) the research is limited to static state of disc and brake interaction. Also, adding thermal residual stresses on crack incurred the need of very high computational power that is not available with current facility. Therefore, thermal effects were evaluated by using fatigue properties at a given temperature.

Experimental analysis is accurate as far as instruments are fully available, sufficient knowledge of using instruments, and good conditions to apply instruments. But due to insufficient time and material unavailability this thesis is not tested experimentally.

1.6 Organization of the Research (Thesis Structure)

The research will be organized in five parts. The first chapter will be the introduction part which clearly states the background of the research, statement of problem, and objective, scope and limitation of the study, clearly states the vehicle braking types, and working principles.

Chapter two: Literature review of the disc brake system of rail vehicle and basic Fracture

mechanics concepts.

Chapter three: Analyses and Modeling i.e. calculate the contact pressure and frictional heat flux.

Chapter four: XFEM Result and Discussion.

Chapter five: Conclusion, Recommendation and Future work.

1.7 Research methods

From the steps of research method, first we collect data, which are important for the work in this paper. Then, Through ought the research, a review of the related literatures is carried out and the gaps are identified. Mathematical analysis of braking is used to determine the applied pressure and heat flux on the disc surface. The CAD model of the disc from SOLIDWORKS software is imported to ABAQUS software and the semi-elliptical surface crack is placed in the disc. Simulations with 4, 8, 12, 16 and 20 mm crack length at normal speed (40 km/hr) and at over speed (80 km/hr) and at room temperature (25 ^{o}C) and at high temperature (500 ^{o}C) are done interchangeably. Finally, the simulation results are illustrated in table and graphically. Based on the results and literature findings, discussion, conclusion, recommendation and future work are given in chapter four and the last chapter.

To fulfil the objectives of the study the following methods in flow chart were used.

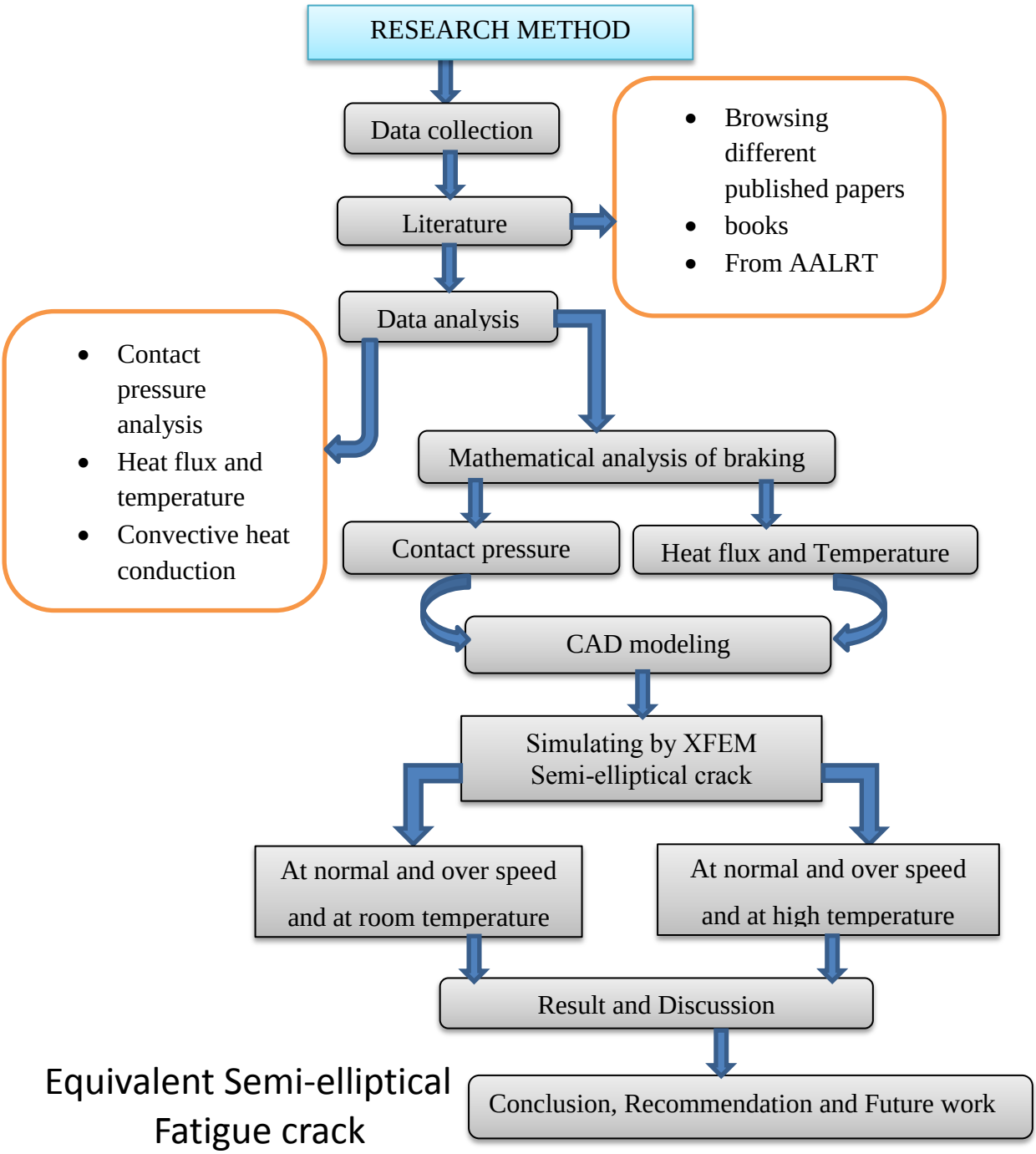

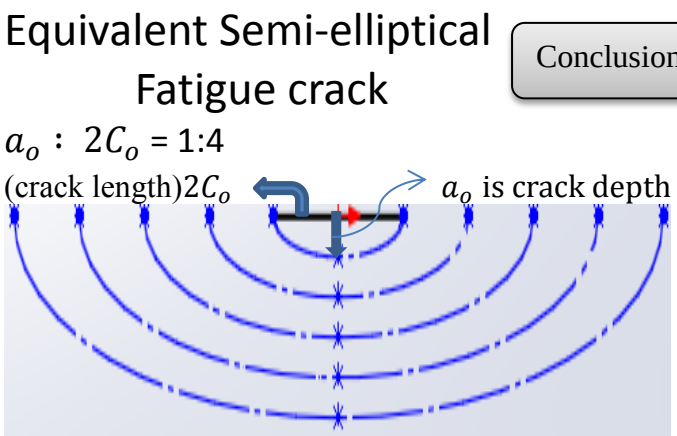

Figure 1-6: Procedure of research

CHAPTER 2 LITERATURE REVIEW

2.1 Introduction

In recent times, disc brakes have increasingly become more popular and gradually found their ways in many different types of vehicles, ranging from light motorcycles to heavy trains. They offer several advantages over drum brakes, including better stopping performance (disc cooled readily), easier to control (not self-applying), less prone to brake fade, and quicker recovery from immersion, which largely contributed to their popularity. However, after long repetitive braking, brake fade could still set in and compromise the performance of a disc brake due to the change of friction characteristics caused by temperature rise and overheating of brake components. Overheated components could further lead to more problems such as thermal cracks, plastic deformation, and premature wear, and the life span of a disc brake could be shortened as a result. Due to the application of brake on the train disk brake rotor, heat generation takes place due to friction and this thermal flux has to be conducted and dispersed across the disk rotor cross section and pad. Due to this great input of heat flux into the disc in a very short time, high temperature difference is produced on the material. Because of high temperature difference the material is exposed to high stress-the consequence is thermal (heat) shock. Rapid aging and fatigues are the result. In addition thermal stresses, mechanical stress also generated on the disc due to rotor force. So, the condition of braking is very much severe and thus the thermal and structural analysis has to be carried out.

The analysis of fatigue crack effect has become increasingly important in product design in different transport means, road vehicles, railway trains, and airplanes. Fatigue crack analysis is a very important stage in the study of braking systems, especially in of railway trains. Cyclic load of braked railway disc brake rotor prevails compared to other type's loads. In the braking phase, kinetic energy is transformed into thermal energy resulting in heating and high temperature states of disc rotor. In case of cyclic loads, which is mainly occur as a result of long-term braking on down-grade railroads and emergency braking, these consequences are the appearance of initiate cracks on the rotor which decrease the rotor braking properties leads to decreases the trains performance.

2.2 Fracture Mechanics

Fracture of material is a big problem that society has faced for as long as there have been man-made structures. The cause of most structural failures generally falls into one of the following categories: Negligence during design, construction, or operation of the structures and application of new design or material, which produces undesirable result [10].

Fracture mechanics is field of solid mechanics that deals with the mechanical behavior of cracked bodies and concerned with the study of the propagation of cracks in material [11]. And crack is a type of fracture that represents solid body in two, or more, pieces under the action of stress in the three major modes: Mode I, Mode II, Mode III or a combination of one and the other [12].

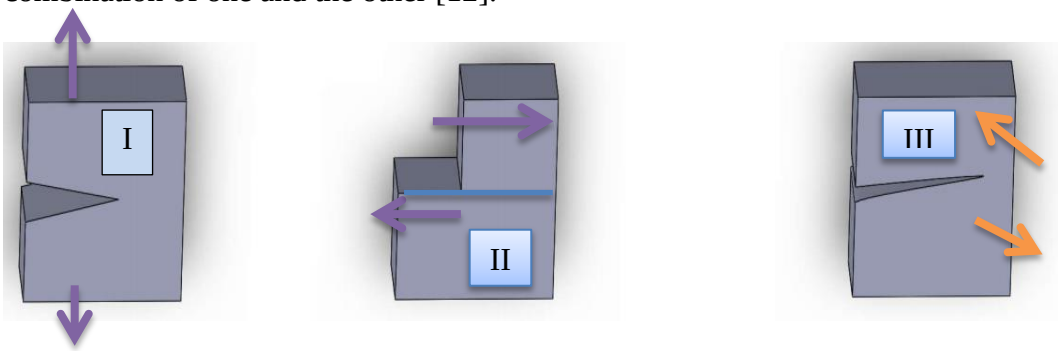

Mode I Mode II Mode III

Figure 2-1: The three loadings of crack: (a) Tension (b) Shear (c) Tearing [12]

In a linear elastic materials, Griffith's approach states that a crack extends if the thermodynamic crack driving force, characterized by the energy release rate G, becomes equal or larger than the crack growth resistance, R (Griffith, 1921) [10][13] where as in 1956 Irwin proposed an energy approach for fracture that is essentially equivalent to the Griffith model, except that Irwin's approach is in a form that is more convenient for solving engineering problems. He postulates that a crack grows when the crack tip stress intensity factor K reaches a critical value K_c.

The Griffith and Irwin criteria are equivalent for linear elastic materials, since energy release rate and stress intensity factor are related. First assumptions taken in LEFM analysis is listed below [10]:

- A sharp crack or flaw of similar nature already exists; the analysis deals with the propagation of the crack from the early stages.
- The material is linearly elastic.
- The material is isotropic.
- The size of the plastic zone near the crack-tip is small compared to the dimensions of the crack.
- The analysis is applicable to near-tip region.

Based on assumption Linear Elastic fracture mechanics (LEFM) is valid only as long as non-linear material deformation is confined to a small region surrounding the crack-tip. In many materials, it is virtually impossible to characterize the fracture behavior with LEFM, and an alternative fracture mechanics model is required.

Elastic-plastic Fracture Mechanics applies to materials that exhibit time dependent, nonlinear behavior (i.e. plastic deformation) [13]. For crack growth in elastic-plastic materials under large scale or general yielding conditions, the common approach is to use criteria based on the crack-tip opening displacement (CTOD) by Wells in 1963, Rice's J-integral in 1968 [10] and the energy dissipation rate by Turner and also Turner Kolednik in 1994.

2.3 Related Literature Reviews

Taking the above in to consideration, many researchers have done brake disc thermo-mechanical coupling analysis, some of them are as follows.

Rehankarim [14], did a research to understand and establish the extent to which train overloading is happening in a developing country like Malaysia by Comparison between actual overloading data for 2- axle, 3-axle and 4-axle trucks and the stopping distance. Because of the author understands the problem of train overloading in developing countries may not fully realized to enable appropriate and effective mitigation measures to be employed. The article also determined the implications of train overloading on safety, simulation data on the stopping distance of different truck categories traveling at different speeds and GVW (Gross Train Weight) was generated using the MSC ADAMS software. Through analysis of the train weight data, namely the GVW was performed to determine the train overloading characteristics at the study location. According to the results from this study Data on GVW violations amongst the different truck types revealed that 50% of the 3-axle trucks are overloaded and the degree of overloading

reaches 101% More than a third of the 4-axle trucks (37%) are also overloaded and degree of overloading reaches 84% of the legal weight limit. As such, the 3-axle and 4-axle trucks may be considered as the main contributors to truck overloading occurrences in Malaysia. Furthermore, even though 9% of the 2-axle trucks are overloaded. And the Malaysian government has spent a large portion of the yearly infrastructure budget on road network and bridge maintenance that causes by overloading. A significant amount of the total allocated budget for road maintenance could be saved if road damage caused by overweight trains can be avoided or at least minimized. The damage on road pavements would be accelerated as the volume of overweight train increases.

Finally the author concludes Significant GVW violation involving overweight commercial trains is observed in Malaysia, The frequency and degree of overloading in heavy commercial trains is very significant and alarming. Not only does overloading accelerate pavement damage (which in turn may contribute to accidents), overloaded heavy trains would be hazardous to other road users. Monitoring and enhancing enforcement of weight limits of heavy trains may be a step in the right direction. And comprehensive and continuous data is needed, especially at critical locations in the road network.

In this study the researcher investigates only the happening of train overload and how much the percentage of it in the country but he does not seen the effect of fatigue crack on disc brake during braking performance and the safety wise of the condition.

Ali and MostefaBouchetera [15] worked on research which consisted on analysis of thermos- elastic behavior of the dry contact between the brake disc and pads in heavy load trains during the brake phase, the researcher uses ANSYS CFX-CFD for the thermal – structural analysis to determine deformation and von misses stress established in disc and contact pressure in pads due to frictional heating affect. The analysis results showed that, temperature field and stress field in the process of braking phase were fully coupled. The temperature, Von Misses stress and the total deformations of the disc and contact pressures of the pads increases as the thermal stresses are additional to mechanical stress which causes the crack propagation and fracture of the bowl and wear of the disc and pads. The result obtained from this simulation is good. But in the modeling and determining of the temperature field in a disc brake during the braking phase they take

only, braking time, increment time and initial time. The researcher is not analyzing fatigue crack propagation of disc brake condition.

Zaid [16] did an investigation of disc brake rotor by finite element. The author has conducted a study on vented disc brake rotor of normal passenger train with full load of capacity. This study is concern of heat and temperature distribution on disc brake rotor. The researcher use finite element method analysis approach for conducted in order to identify the temperature distribution and behavior of disc brake rotor in transit response. ABAQUS/CAE has been used as finite elements software to perform the thermal analysis. The author concludes the maximum temperature of transit response is 543.9 ^{O}C and where the temperature range of gray cast iron which is between -150 ^{O}C and 550 ^{O}C, so the author expected that all findings in this study will.

Kumella [17] did a work on determining nodal temperature and friction coefficient considering different loading and operating conditions of Addis Ababa light rail train (AALRT). The research uses finite element method analysis approach for conducted in order to identify the temperature distribution and behavior of disc brake rotor in transit response at selected site and Multi-physics ANSYS work bench 14.5version has been used to evaluate thermal analysis under service and emergency braking condition independently. The researcher concluded the performance of disc brake is highly affected during emergency braking condition due to minimum stopping distance and delay time. The maximum nodal temperature is 413.88 ^{O}C which is much less than from the allowable values of 800 ^{o}C.

Li et al. [18] worked a research to investigate the mechanism of crack formation on the brake discs in service on china railway high-speed (CRH) rolling stock. The effect of operating conditions on crack propagation was studied by analyzing three cases: (1) emergency brake applications from the initial velocity of 300 km/hr, (2) emergency brake applications from the initial velocity of 200 km/hr and service brake applications from the initial velocity of 200 km/hr, where regenerative braking played a significant role in the total braking performance. At the first case scenario of analysis, a brake disc, which was subjected to emergency brake applications from the initial velocity of 300 km/hr, was dismantled from the motor axle. The length of the cracks exceeded the limit permitted by maintenance rules; therefore the disc was withdrawn from service. The

second scenario was investigated by the full-scale dynamometer testing around 1000 emergency brake applications were performed. The third case was studied by monitoring the brake discs operating in normal service for six months, which resulted in approximately 8000 service brake application. No emergency brake applications were performed during this period. The authors analyzed overheated areas and fatigue cracks evolution by comparing the photographs. The distinction has been made between crackles, i.e. network of superficial material discontinuities and cracks, i.e. deep and long fractures.

Five samples were cut out from brake discs that were subjected to emergency brake applications from the initial velocity of 300 km/hr. The specimens were fractured along the cracks and their geometry was analyzed. The cracks were half-elliptic in shape and their maximum depth was between 4.0 and 5.4 mm. it was found that the fatigue cracks propagated mainly in radial direction. Hardness was measured at several points along the thickness of the disc. Furthermore, the microstructure of the material was examined which indicated a phase change in the disc material in the overheated areas. Finally, elemental analysis of the areas in the close vicinity of the cracks indicated substantial oxidation concerning brake disc subject to emergency brake applications from the initial velocity of 300 km/hr, while the areas close to the fatigue cracks on the brake disc subject only to service brake applications from the initial velocity of 200 km/hr were not oxidized. It was concluded that increase in braked energy leads to conditions more favorable in terms of crack propagation. The simulation was performed by transient Finite element analysis to calculate temperature fields in the course of brake applications.

Zhang, Wu et.al [19]**,** did an investigation to evaluate fatigue life and safety domain of in-service of high speed train disc brake at 400 km/hr initial speed. The research uses Extended Finite Element Method (XFEM) and crack tip region meshing refinement, a semi-elliptical surface crack was then inserted into a predicted macroscopic hot spot to carry out the thermal fatigue cracking analysis under consecutive emergency braking. The author determines the peak temperature (681.2 ^{o}C) and calculated crack geometry were well in agreement with experimental and also determines number of emergency brake cycle times (277,179) and maximum crack tip principal stress at 132 mm (1424.3 Mpa). However, the author was only taking at 400 km/hr initial speed and not showing the effect of speed and temperature in fatigue crack growth.

YANG [20], worked on research thermal fatigue life evaluation method of brake disc of high speed train with new materials based on the experimental study and the finite element computation. The aluminum alloy of SiCp/A356 composite was used to verify this research. The author analyzed crack propagation law of cracked fatigue specimens under the thermal load and the relationship of the crack propagation rate and the crack length of SiCp/A356 was gained which could be used to predict the fatigue life of crack propagation.

Summary of the Reviewed Literature:

A literature reviews conducted above to investigate the past research that has been done in many areas related to this work are reviewed. In addition, description, methods, results of the literatures are discussed. The limitations and strengths of the research (validation of the results) were analyzed. Most of the literatures listed in this thesis focus only the thermo-mechanical analysis of disc brake due to heat flux generated on the disk either from kinetic energy of the vehicle, moment of inertia, or centrifugal load of the vehicle. In this thesis the thermomechanical analysis of fatigue crack propagation of disc brake due to both kinetic energy and potential energy at room temperature (25 ^{o}C) and high temperature (500 ^{o}C) during emergency braking for both normal and over speed will be analyzed AALRT.

Although the objectives of the above-mentioned study differ from the objective of this project, similarities can be drawn in the simulation set-up. For instance, the proportion of heat entering the disc as well as the convective heat transfer coefficient can be used as a reference for this thesis. However, the idea of using a PC based program to calculate crack propagation inputs is novel and can be used in this thesis to calculate the thermal parameters as well.

CHAPTER 3 ANALYSIS AND MODELLING

3.1 Thermo- Mechanical Analysis of rotor disc brake with Analytical Method

During the Mechanical and Thermal load computations, the basic boundary conditions are taken from the data of Addis Ababa Light Rail Transit system of the Ethiopian Railway Corporation as a case study. The Material properties that can never be found in the LRT project were taken from different published papers which are cited along with them.

Table 3-1: Seating capacity of the train [21]

Number of passengers (persons)	Seated	Standing	Total
Seats (AW_1)	65	**0**	65
Seating capacity (AW_2) (standing: 6 persons/m^2)	65	189	254
Overload capacity (AW_3)(standing: 8 persons/m^2)	65	252	317

Table 3-2: Weights of the train [21]

Loads	Car body weight	Passenger weight	Total weight
Empty vehicle (t)	44	0	44
Seating capacity (t)	44	15.24	59.24
Overload capacity (t)	44	19.02	63.02

Note: Take 60kg as average weight of each passenger.

3.1.1 Main Technical Parameter [21]

I. Speed

Maximum operation speed: 80 km/h

Average travelling speed: ≥ 20 km/h (average dwelling time of 30 seconds at each station)

II. Average acceleration [21]

Under rated load and rated voltage on straight and dry track, with half-worn wheels, average acceleration is as below:

Train speed from 0km/h to 40 km/h ≥1m/s^2

Train speed from 40km/h to 80 km/h ≥0.5m/s^2

III. Average Braking Deceleration [21]

Under rated load on straight and dry track, with half-worn wheels, average deceleration from maximum train operation speed of 80 km/h until stop is as below:

Maximum service brake deceleration: ≥1.1m/s^2

Emergency brake deceleration: ≥2.0m/s^2

IV. AALRT Train Brake System Description

Table 3-3: Type of brake and mounting place [21]

Abbreviation	ED	EHM	EHT	MTB	Sanding
Type	Electric brake, Generally depending on load	Hydraulic Brake of Motor Car	Hydraulic Brake of Trailer Car	Magnetic track brake	Sanding device
Mounting place	M1 + M2 Motor bogie for M1 + M2	M1 + M2 Motor bogie for M1 + M2	TB1 Trailer bogie for TB1	M1 + M2 + TB1	M1 + M2 Motor bogie for M1 + M2

Table 3-4: Type of brake and way of application [21]

Brake system	Service brake (Maximum)	Emergency brake	Safety brake	Stopping brake	Holding brake	Parking brake
ED-Brake	✓	✓				

EHM-Brake		✓	✓	✓	✓	✓
EHT Brake	✓	✓	✓	✓	✓	
MTB Brake		✓	✓			
Sanding		✓	✓			

Note: ✓ indicates way of brake application in such brake mode.

V. AALRT Train Service Brake

During Service brake will be activated when driver controller is in brake position. Brake set point is linearly proportional to handle position. ED brake is major brake type for motor car and takes precedence over EH brake. Regenerative brake is applied preferably as electric brake. When train brake cannot be satisfied by ED brake under all speed and load conditions, EH brake of trailers will furnish extra brake based on blended functions. At low speeds (up to 5km/h), electric brake will descend while hydraulic brake will ascend. However, total braking force remains unchanged. Service brake is limited to load correction and jerk.

VI. AALRT Train Emergency Brake (ED + EH + MG brake)

For emergency brake, ED brake for motor car and EH brake and magmatic brake for trailer will operate simultaneously. Emergency brake is not limited to jerk after load correction.

[Source: Addis Ababa (E-W and N-S) rout light rail transit train technical specification from ERC, September 2009].

3.1.2 Thermal Transient Analysis of the Disc Brake

For an isotropic material with internal heat generation, the governing equations for 3D heat conduction equation under transient conditions in Cartesian coordinate systems are as follows below:-

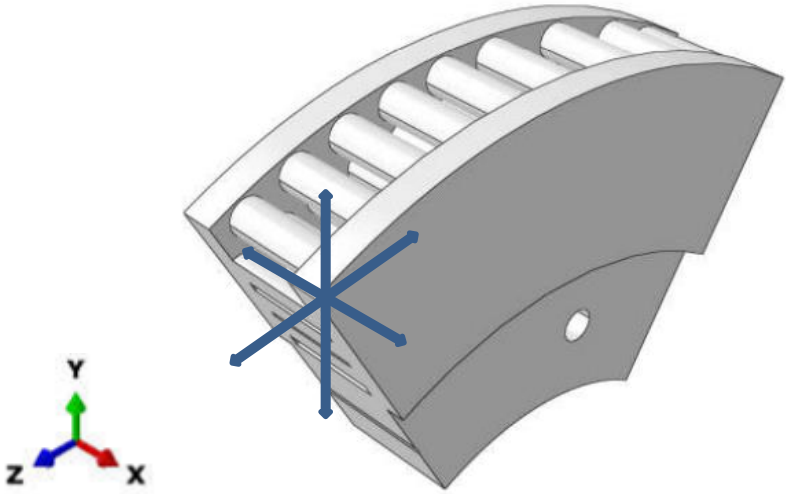

Figure 3-1: Three-dimensional heat conduction through a disc volume element

$$K_x \frac{\partial^2 T}{\partial X^2} + K_y \frac{\partial^2 T}{\partial Y^2} + K_z \frac{\partial^2 T}{\partial Z^2} + Q = \rho C_p \frac{\partial T}{\partial t}, \quad \textbf{Eq. 3.1}$$

where K_x , K_y , and K_z are thermal conductivity in x, y z-directions, respectively, C_p is the specific heat , ρ is the specific mass, Q is internal heat generation rate per unit volume and T is the temperature that varies with the coordinates as well as time t.

Heat conduction in any direction within the material is governed by Fourier's law of heat conduction is:-

$$q = - kA\frac{dT}{dX}. \quad \textbf{Eq. 3.2}$$

In transient thermal analysis requires material properties which include thermal conductivity, specific heat and density. An isotropic material has the same properties in every direction. The boundary conditions are specified by the heat flux entering the model and dissipated from the model and dissipated from the model by convection or radiation. The initial conditions are specified by the initial nodal temperature value. The heat transfer rate of convection for the disc brake dominates the cooling process specified by Newton's law cooling:-

$$q_s = - k\, h(T_S - T_\infty) \text{ where } T_S = T_1(X, Y, Z), \quad \textbf{Eq. 3.3}$$

where: h – convective surface heat transfer coefficient (also known as the film conductance)

T_1 –specified surface temperature,

q_s –specified surface heat flux (positive into a surface),

T_s –Unknown surface temperature and T_∞ -convective exchange temperature.

3.2 Numerical Model of Disc Brake

During brake application is defined as an application of the brake that results in a brake force being applied to the train. Brake force is the force applied to the brake disc /pad/ braking surface interface [22].

Railway locomotive running with initial velocity (V_o) is assumed to stand still with constant deceleration (a). Its linear translational velocity as function of time (t) is given by:

$$V(t) = V_o \ . \qquad \textbf{Eq. 3.4}$$

The angular velocity (ω) of the wheel set can be determined as follows:

$$\omega(t) = \frac{V(t)}{r_w}, \qquad \textbf{Eq. 3.5}$$

$$\omega_o = \frac{Vo}{r_d}, \qquad \textbf{Eq. 3.6}$$

where:

V-velocity of the locomotive,

V_o –initial running velocity of the locomotive,

ω_o –initial angular velocity the wheel,

ω –angular velocity of the wheel at any time,

r_d –the radius of disc.

During the application of brake, the brake force acts at the effective radius (r_{disc}) of disc rotor and translational velocity (V_{disc}) of this frictional force (F_{disc}) could be expressed in terms of the translational velocity $V(t)$ of the locomotive as follows.

$$V_{disc} = \frac{r_{disc}}{r_w} V(t). \qquad \textbf{Eq. 3.7}$$

The total braking time and distance can be calculated by the formula:

$$S_b = V_o t_b - \frac{1}{2} a t_b^2 \ , \qquad \textbf{Eq. 3.8}$$

$$t_b = \frac{V_o}{a} \ . \qquad \textbf{Eq. 3.9}$$

Hence, angular velocity (ω) at any time (t) could also be determined as follows:

$$\omega = \omega_o \ (1 - \frac{t}{t_b}), \qquad \textbf{Eq. 3.10}$$

where:

t_b –braking time to stop the locomotive,

S_b –total brake distance.

Initial velocity and mass of train are belongs to the factor which affects the total braking distance and braking time. The braking distance and time increase when velocity increases. This is explained by the relation between kinetic energy and velocity. The greater the velocity the greater kinetic energy the brakes have to transfer. Mass of the vehicle is also related to kinetic energy in relationship. The greater the mass the greater kinetic energy, thus a heavier train will require a longer braking distance and time.

Both braking time and braking distance changes with the velocity of the train changes. The train going uphill gravity assists and reduces the braking time. Similarly, gravity works against when train are descending and will increase the braking time give a constant deceleration. The paper takes the same velocity of a train (80km/h) on level and gradient track position in time of emergency and service brake and constant deceleration (for service brake 1.1m/s^2 and emergency brake 2m/s^2) in both track positions. That is why the braking time in gradient and level track condition in the calculation of this paper is equal

3.2.1 Analysis of Disc Rotor Force

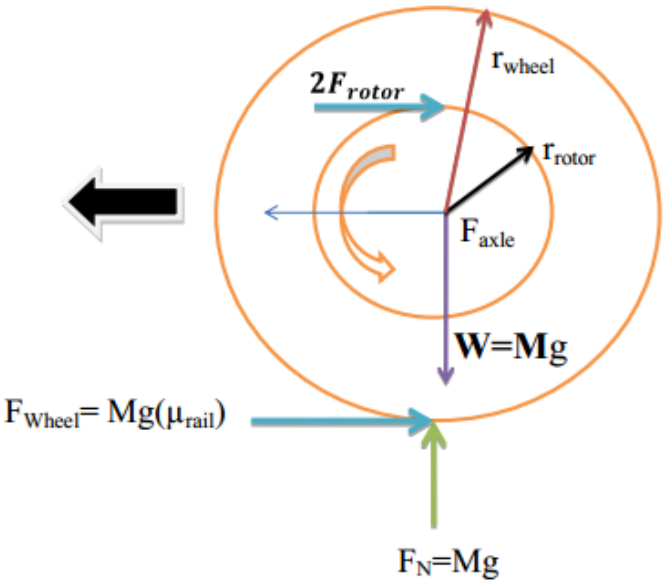

Figure 3-2: Free body diagram of wheel rotor system

3.2.2 Train Braking Energy at Level or Horizontal Track

When the train is applied brake on the flat surface, the brake force have only oppose kinetic energy of the train because the train potential energy is neglected as downhill of the train is set to be zero. Due to this kinetic energy heat is developed between disc and pads. Braking energy during this time is equals to the train kinetic energy ($K_E = E_b$).

$$K_E = \frac{1}{2}mv^2. \quad \textbf{Eq. 3.11}$$

The train has also many rotating components, so that it has a rotational kinetic energy due to rotating parts. Then the heat energy equation will be:

$$K_E = \frac{1}{2}MV_o^2 + \frac{1}{2}I\omega_o^2 , \quad \textbf{Eq. 3.12}$$

where:

K_E –initial kinetic energy of the locomotive just before braking starts,

M –mass of locomotive,

I –polar inertial moment of rotating parts.

And, the moment of inertia of the rotating wheel set and discs can be calculated by using the equation, is given by:

$$I = \sum_{i=1}^{n} m_i r_i^2, \quad \textbf{Eq. 3.13}$$

Where:

m_i –represents the masses of the wheel set and brake discs,

r_i – represents the rotation radius of the rotating parts from the center of rotation.

In this case, all the rotating parts are fixed on the axle of the wheel set and the rotation axis could be taken as the tangent line joining the contact point of the rail heads with wheel set of the locomotive. It is the parallel to the axis of the wheel axle. Hence, the rotating radius is and equal to the radius of the wheel (r_w). Hence,

$$K_E = \frac{1}{2}MV_o^2 + \frac{1}{2}I\omega_o^2 = \frac{1}{2}MV_o^2\left[1 + \frac{1}{Mr_w^2}\right] = \frac{1}{2}(1.1)MV_o^2. \quad \textbf{Eq. 3.14}$$

The term $\left[\frac{1}{Mr_w^2}\right]$ accounts to the rotational masses involved and its value equals 0.1. In some literatures, the contribution of the rotating masses of the wheel set and discs is

taken to be 10% the tare weight of the axle load of locomotive[23]. Therefore, the total braking energy when the trains travel in horizontal track is

$$K_E = \frac{1}{2}(1.1)MV_o^2. \quad \textbf{Eq. 3.15}$$

3.2.3 Brake Force at Level or Horizontal Track

When the locomotive begins to brake due to this the train lost power and will stop by frictional forces. The imposed mechanical energy theoretically transformed to frictional heat.

The brake disc rotor has got two friction surfaces ($2A_b$) swept by the brake pads on both sides and two friction forces ($2F_{disc}$) act on both faces of the disc at an effective radius (r_{disc}). These forces retard the movement of the locomotive.

The total heat flux is equal to = $\frac{Total\ heat\ generated}{braking\ time * twice\ the\ projected\ area}$.

$$\text{Total heat flux} = \frac{Q_g}{2A_b * t_b} = \frac{E_b}{2A_b * t_b}, \quad \textbf{Eq. 3.16}$$

where:

A_b – is the area swept by the brake pad at one face of the disc

The total work of friction force during the whole brake cycle equals with the total heat generated.

$$Q_g = E_b = \int_0^{t_b} P(t)dt, \quad \textbf{Eq. 3.17}$$

$$\frac{1}{2}(1.1)MV_o^2 = (2F_{disc})\int_0^{t_b} V_{disc}(t)\,dt, \quad \textbf{Eq. 3.18}$$

$$\frac{1}{2}(1.1)MV_o^2 = (2F_{disc})\frac{r_{disc}}{r_{wheel}}\left[V_o t_o - \frac{1}{2}at_b^2\right], \quad \textbf{Eq. 3.19}$$

$$F_{disc} = \frac{\frac{1}{2}(1.1)MV_o^2}{2\frac{r_{disc}}{r_{wheel}}\left[V_o t_o - \frac{1}{2}at_b^2\right]}. \quad \textbf{Eq. 3.20}$$

3.2.4 Heat Generated During Braking at Downhill Gradient

In braking system the applied mechanical energy is transformed in to heat energy and thus generated heat energy range between the pad and disc is determining the braking efficiency of the system. The energy dissipated in the form of heat can generate in temperature range from 300 ^oC to 800 ^oC [24].

Total heat generated (Q_g) in the brake system equals the total braking energy (E_b) lost from the locomotive during braking.

$$Q_g = E_b \,. \qquad \textbf{Eq. 3.21}$$

3.2.5 Braking Force of a Train on Downhill Motion at Train Downhill Position

During the train begins to apply brake, the train cut the power supply and will stop by frictional forces. The imposed mechanical energy theoretically transformed to frictional heat.

In interaction of disc and pad, brake disc rotor has got two friction surfaces ($2A_b$) swept by the brake pads on both sides and two friction forces ($2F_{disc}$) act on both faces of the disc at an effective radius (r_{disc}). These forces retard the movement of locomotive.

The total heat flux is = $\frac{Total\ heat\ generated}{twise\ pad\ and\ disc\ friction\ area * braking\ time}$,

$$\text{Total heat flux} = \frac{Q_g}{2A_t * t_b}\,, \qquad \textbf{Eq. 3.22}$$

where:

A_b –area swept by the brake pad on one face of the disc,

T_b –braking time.

Total work of friction force during the whole brake cycle equals with total heat generated.

$$Q_g = E_b = \int_0^{t_b} P(t)dt, \qquad \textbf{Eq. 3.23}$$

$$\frac{1}{2}(1.1)MV_o^2 + \text{M.g.S}_b \frac{\delta}{1000} = (2F_{disc})\int_0^{t_b} V_{disc}(t)\,dt. \qquad \textbf{Eq. 3.24}$$

$$\frac{1}{2}(1.1)MV_o^2 + \text{M.g.S}_b \frac{\delta}{1000} = (2F_{disc})\frac{r_{disc}}{r_{wheel}}\left[V_o t_o - \frac{1}{2}at_b^2\right]. \qquad \textbf{Eq. 3.25}$$

The friction force that work on the disc to retard the locomotive on train downhill position is given by:

$$F_{disc} = \frac{\frac{1}{2}(1.1)MV_o^2 + \text{M.g.}S_b\frac{\delta}{1000}}{2\frac{r_{disc}}{r_{wheel}}\left[V_o t_b - \frac{1}{2}at_b^2\right]}. \qquad \textbf{Eq. 3.26}$$

In this paper, considering the amount of heat generation by wear is very small relative to the heat generated by friction, so the effect of material wear is neglected. Therefore, using the value of the frictional force obtained above, the transient heat flux can be

determined. The heat power generated at the effective radius (r_{disc}) of the disc can be expressed as follows:

$$Q(t) = (2F_{disc})\, V_{disc} = 2F_{disc}\ \frac{r_{disc}}{r_{wheel}}(V_o - at). \qquad \textbf{Eq. 3.27}$$

3.2.6 Heat Flux Entering the Disc

The thermal analysis of the braking system of railway trains requires determination of the quantity of heat produced by interaction of disc and pad due friction, as well as the distribution of this energy between the railway disc and the braking pads.

Totally, the thermal conductivity of the material of the brake force pads is lower than that of the disc ($K_P < K_d$). Because the disc material gray cast iron with high carbon content has good thermos-mechanical characteristics. The brake pad has an isotropic elastic behavior so considering 95% of the heat quantity produced will be completely absorbed by the brake disc [25].

3.3 Material Properties of Gray Cast Iron

Brake disc are normally made of cast iron. The reason this material is used is generally thought to be because of its low cost, ease of manufacturing, strength, and resistance to thermal loading [26]. The AALRT train disc brake also constructed from gray cast iron, So for the transient analysis of the passenger train disc brake certain physical properties of gray cast iron are given below [25]. However, to get the exact material property of AALRT disc brake is difficult due to it we use the most related material.

Table 3-5: Material properties of gray cast iron [27]

Material properties	**Disc**
Density $[kg/m^3]$	7250
Poison's ratio	0.28
Thermal conductivity $[W/m.k]$	57
Specific heat capacity $[J/kg.k]$	447
Compressive ultimate strength $[Mpa]$	820
Tensile ultimate strength $[Mpa]$	240
Yield stress $[Mpa]$	400
Thermal expansion $[\mu m/m.k]$	10.85
Elastic modulus E $[Mpa]$	138

The ratio normally is called the proportion of heat transferred to disc ($\gamma = 0.95$). The rate heat generation is given by:

$$\dot{Q_d}(t) = \gamma(2F_{disc})\, V_{disc} = (0.95)(2F_{disc})\frac{r_d}{r_w}(V_o - at). \quad \textbf{Eq. 3.28}$$

Now focus on the railway disc rotor that most of heat generated is characterized by the heating of the disc. The heat conduction in the disc is governed by the classic heat equation is given by:

$$\rho C_P\, \dot{T} = k\sum_{i=1}^{3}\frac{\partial^2 T}{\partial X_i^2}, \quad \textbf{Eq. 3.29}$$

where:

P –Density for material of the disc,

k- Thermal conductivity,

C_P – Specific heat capacity.

At the contact surface between the brake disc and pads produce heat during the braking process. According to the expression below the heat dissipation from the free surface of the disc to the surrounding air is described by both convection and radiation as follows:

$$Q_{disc} = -h(T - T_{ref}) - \varepsilon\,\sigma(T^4 - T^4_{ref}). \quad \textbf{Eq. 3.30}$$

In this equation:

h -Convection film coefficient,

ε –material's emissivity,

σ –Stefan-Boltzmann constant,

T_{ref} –temperature of the surrounding air.

The effect of radiation heat transfer is not considered because it is less important especially for the law surface temperatures due to thus, the primary mean of heat rejection between air and brake rotor surface is done by convection [28].

At the brake disc rotates at high speed, the convection coefficient of the brake disc changes with the disc speeds during braking. For convection heat exchange based on convection heat transfer theory, the convective film coefficient between outer brake surface and air as a function of the railway vehicle velocity, the following formula should be used.

$$h = \frac{0.037 \times K_{air}}{2r_b} Re^{0.8} \times Pr^{0.33}. \quad \textbf{Eq. 3.31}$$

Reynolds and Prandtl number are given respectively Re and Pr by the following formula

$$\text{Re} = \frac{2\rho_{air} \times V_{rail} \times r_b}{\mu_{air}}, \quad \textbf{Eq. 3.32}$$

$$Pr = \frac{C_{air}\mu_{air}}{K_{air}}, \quad \textbf{Eq. 3.33}$$

where:

K_{air} –conductivity of air (0.0241w/mK),

V_{rail} –railway speed,

μ_{air} –Dynamic viscosity of air (12.34×10^{-6} m^2/s),

C_{air} –specific heat capacity,

r_b – Effective friction radius.

The Reynolds and Prandtl number is equals to:

$$\text{Re} = \frac{2\times1.184\times0.1765\times22.22}{12.34\times10^{-6}} = 0.753\times10^6,$$

$$Pr = \frac{1009\times12.34\times10^{-6}}{0.0241} = 0.517.$$

Finally heat convection coefficient is equal to:

$$\text{h} = \frac{0.037\times0.0241}{2\times0.1765} \times (0.753 \times 1000000)^{0.8} \times (0.517)^{0.33} = 102.17 \text{ w/m}^2\,^{o}\text{C}.$$

Therefore, heat transfer coefficient of the disc is equals to, h =102.17 w/m^2 ^{o}C. By the end the first emergency braking action the disc temperature has reached 503.46 ^{0} C as shown on Figure 3-5 due to friction. The train then stops at station for 30 second (average station dwelling time of AALRT) and the train starts to move to the next station with two different acceleration values (a_1 =1.0 m/s^2 and a_2 = 0.5m/s^2) up to the maximum speed. The first acceleration is 1.0m/s^2 up to a speed of 40 km/h (11.11m/s) and then up to the final velocity using 0.5m/s^2 acceleration (according to AALRT technical specification). And then the next braking action starts. The total time for cooling of the disc is the summation of the times stopping at station and the time required to reach to the top speed.

$$t = t_s + t_{a1} + t_{a2} = 30 + 28.71 = 58.71,$$

where:

t –total time,

t_s–station stopping time,

t_{a1} –time for the first acceleration,

t_{a2} –time for the second acceleration.

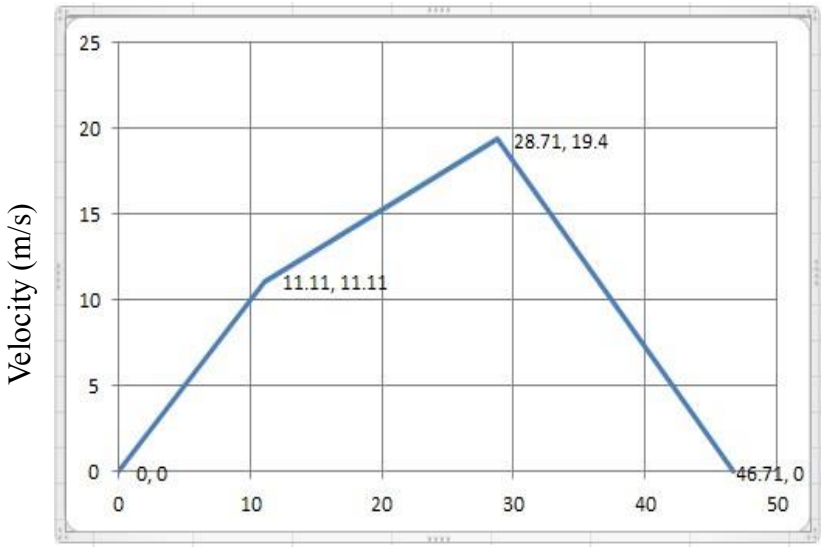

Figure 3-3: velocity vs. time graph

So the total cooling time of the disc is equal to 59 seconds.

3.4 Initial Temperature of Disc for the Next Braking

After the first braking, the initial temperature of the disc is rises above from its ambient temperature and it will be computed according to Newton's law of cooling is described by:

$$T = T_\infty + [(T_1 - T_\infty) \times \left[exp - \frac{hA}{mC} \times t\right]], \quad \textbf{Eq. 3.34}$$

where:

T –cooled temperature,

T_1 –maximum temperature,

T_∞ -ambient temperature,

A –disc brake contact area,

h –heat transfer coefficient,

t –total cooling time,

m –mass of disc,

C –specific heat capacity of gray cast iron.

In this paper, the initial temperature for the next braking action is calculated by the service brake unacceptable load thermal result obtained (489.7 ^{o}c).

$$T = 30 + [(503.46 - 30) \times \left[exp - \frac{84.36 * 0.0752}{39.4 * 447} \times 59\right]],$$

$$= 480\ ^{o}c.$$

3.5 Determination of Locomotive Load Condition

The specific loading condition during in this analysis is braking of the locomotive running with a maximum velocity of 80 km/h to standstill with temperature of the surrounding is 30 ^{o}c. The assumed temperature is average environmental temperature of the operating route of the locomotive in the region. In addition, the part of the track with a gradient of 5.5% is also considered.

Hence, the initial temperature of the disc and the surrounding is the same (30 ^{o}c). The main purpose is to find out how much temperature distributed on the whole construction of the disc brake rotor by braking on the inclined and horizontal track. The deceleration factor for service brake and emergency brake are 1.1m/s^2 and 2.0m/s^2 respectively.

In both cases the effect of the humidity in the air and the heat transfer with radiation is not considered due to small influence.

3.5.1 Weight Transfer during Braking Condition

During a locomotive is standing still on straight track, its weight is uniformly distributed on all axles. On application of brakes on the train, inertia forces are setup. The braking force is applied at lesser height where as the train load is at a higher height.

According to SF6N bogie weight transfer mechanism, the weight transfer efficiency of SF6N (WWAG6C) has been 97.4%.

Therefore, equal and uniform weight distribution among the front and rear axles of the bogie is considered in this paper.

3.6 Physical Model of Disc Brake

Weight distribution of the locomotive is supposed equally distributed between on both the front and rear bogies. Each bogie consists of two wheel sets and every wheel set is equipped with one wheel mounted mechanical disc brakes on trailer bogie. And one mechanical disc brake on motor bogies axle. Hence, only 1/8 of the whole brake force is applied to one disc from the trailer part of the carriage and 1/6 on motor bogies disc brake. The braking energy for one wheel considering train horizontal track position is given below:

$$\frac{1}{8}\left[\frac{1}{2}MV_o^2(1.1)\right] = (2F_{disc})\int_0^{t_b} V_{disc}\ \mathrm{dt}. \qquad \textbf{Eq. 3.35}$$

The braking energy for one wheel considering train deceleration position as follows:

$$\frac{1}{8}\left[\frac{1}{2}MV_o^2(1.1) + \mathrm{M.g.}\ S_b\ \frac{\delta}{1000}\right] = (2F_{disc})\int_0^{t_b} V_{disc}\ \mathrm{dt}. \qquad \textbf{Eq. 3.36}$$

This change of energy is equal to the heat flux on the surface of the disc. This ratio is used to calculate the thermal load on the brake disc. Other operational data used for the analysis are listed in table below.

Table 3-6: Data for calculating heat flux

Input Parameter	**Values**
Mass of the train –M[kg]	63020
Velocity –$V_o[m/s]$	22.22
Deceleration for service brake –a $[m/s^2]$	1.1
Deceleration for emergency brake –a $[m/s^2]$	2.0
Service braking time –t_b [s]	17.67
Emergency braking time –t_b[s]	11.11
Radius of the wheel –r_w [m]	0.33
Incline of the track – δ [%]	5.5

Coefficient of friction has significant effect on the thermal field of interaction between pad and disc. The value of the coefficient of friction depend on numbers of tribological parameter such as speed of relative movement of parts in contact, the contact surface roughness, quality of materials of a tribo-pair, temperature of contact parts and so on [29]. However, this paper did not consider tribological parameters of braking processes. According to DIN EN ISO 1183 the value μ = 0.36 of the friction coefficient for materials of the disc and the pad for locomotives is taken as the recommended value.

3.7 Determination of the Friction Surface and Parameters of Disc and Pad

Based on UIC 541-3 standard, a sinter material brake pad and gray cast iron disc with dimension tabulated in table below is used to calculate friction swept area on the disc by the brake pad.

Table 3-7: Dimension of disc and brake pad for railway locomotives

Description of parts	**Disc**	**Pad**
Outer radius (R_o), [m]	0.210	0.210
Inner radius (R_i), [m]	0.143	0.143
Bolts hole Radius [mm]	(ϕ12*9)	-
Inner bore radius [mm]	0.90	-
Friction face thickness (L), [M]	0.012	0.011
Effective friction radius (r_b), [m]	0.1765	-
Friction surface (A_b, A_p), [m^2]	0.0752	0.0125

Effective radius of study is the intermediate friction surface radius of the disc r_b = 0.1765m. The calculated contact surface area between the disc rotor and braking pad is $A_b = 0.0752m^2$.

3.7.1 Determination of the Load on a Disc

The value of force which works for one brake disc in train horizontal position is described by:

$$F_{disc} = \frac{\frac{1}{8}[\frac{1}{2}MV_O^2(1.1)]}{2\frac{r_{disc}}{r_{wheel}}\left[V_o t_b - \frac{1}{2}at_b^2\right]}. \quad \textbf{Eq. 3.37}$$

The value of the friction force which work for one brake disc at train deceleration position is given by:

$$F_{disc} = \frac{\frac{1}{8}\left\{\frac{1}{2}MV_O^2(1.1) + M,g\left[V_o t_b - \frac{1}{2}at_b^2\right]\frac{\delta}{1000}\right\}}{2\frac{r_{disc}}{r_{wheel}}\left[V_o t_b - \frac{1}{2}at_b^2\right]}. \quad \textbf{Eq. 3.38}$$

3.7.2 Pressure determination for the brake caliper

The surface pressure between the disc and pad, on behave of the calculated force applied on the disc, needs to be determined. The pressure force which works for one brake disc is:

$$P_{disc} = \frac{F_{disc}}{2A_{b*\mu}}, \quad \textbf{Eq. 3.39}$$

3.7.3 Data for Train Acceptable Load Condition

Calculated and collected data about emergency brake are listed below.

Table 3-8: calculated and collected emergency brake data at 40 km/hr

Service brake			
Brake in horizontal track		Brake in downhill	
Description	Value	Description	Value
Braking time , t_b [s]	5.56	Braking time , t_b [s]	5.56
Deceleration, a $[m/s^2]$	2	Deceleration , a $[m/s^2]$	2
Heat flux/disc Q [W]	5116188.99	Heat flux/disc Q [W]	5117443.74
Pressure/ disc P [pa]	251453.34	Pressure/ disc P [pa]	251515

Table 3-9: calculated and collected emergency brake data at 80 km/hr

Emergency brake			
Brake in horizontal track		Brake in downhill	
Description	Value	Description	Value
Braking time, t_b [s]	11.11	Braking time, t_b [s]	11.11
Deceleration –a $[m/s^2]$	2.0	Deceleration –a $[m/s^2]$	2.0
Heat flux/disc Q [W]	10241588.05	Heat flux/disc Q [W]	10367951.86
Pressure/ disc P [pa]	251492.69	Pressure/ disc P [pa]	254595.71

The above calculated values are used for the ANSYS and ABAQUS analysis.

Finite Element Mesh

Different mesh size like course, medium and fine mesh were considered too improve the mesh quality. Out of different mesh size fine mesh were considered.

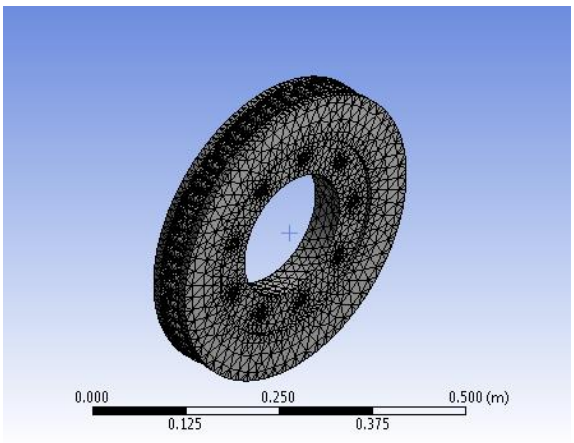

Figure 3-4: Meshing of Disc in ANSYS

Thermal Analysis Result

The result shows 503.46 ^{o}C on the disc surface due to the application of braking during the interaction of disc brake and pad which is less than from the allowable values of 800 ^{o}C. This temperature is used to determine crack propagation behavior of disc at 503.46 ≈500 ^{o}C

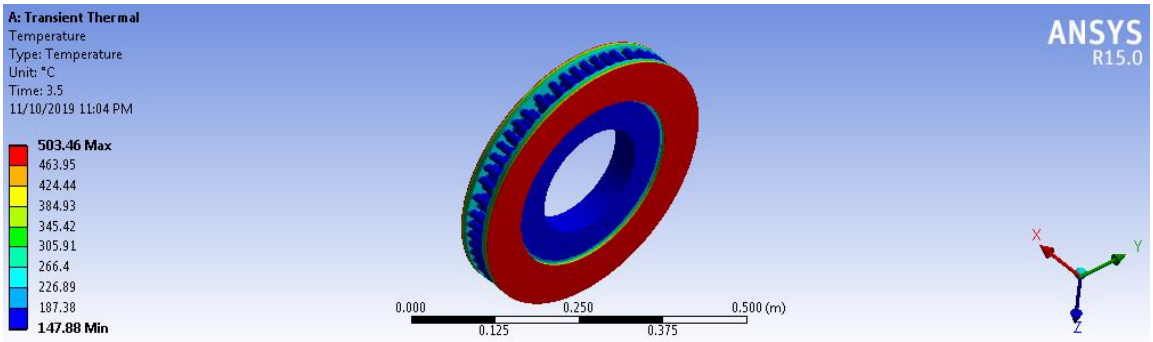

Figure 3-5: Emergency braking in downhill and recommended load condition

It is well-known that thermos-physical properties of material change sharply around the hot spots, which inevitably causes the stress concentration and thermal cracks after several thousand miles. Experimental results show that thermal fatigue cracks initiate from the largest hot spot and then steadily propagate along the radial direction of brake discs under repeated high thermal gradients [19]. It is thus reasonable to insert a crack on disc surface of high temperature gradient.

At elevated temperatures, these cracks then continue to propagate rapidly along the radial direction of the brake disc surface [30], as illustrated in figure below.

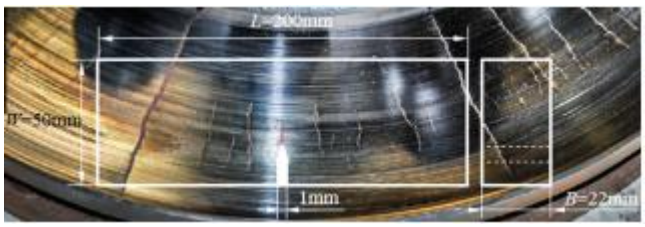

Figure 3-6: The schematic picture of the SEB on a thermal fatigue cracked brake disc

3.7.4 Calculation of Effective Stress Intensity Factor

Tanaka [31] provides the expression of the range of effective stress intensity factor range for a multiaxial fatigue crack as follows:

$$\Delta K_{eff} = \left[(\Delta K_I)^4 + 8(\Delta K_{II})^4 + \frac{8(\Delta K_{III})^4}{1-v}\right]^{1/4}, \quad \textbf{Eq. 3.40}$$

where: $\Delta K_I = \Delta K_{I\,max} - \Delta K_{I\,min}$,

$\Delta K_I = \Delta K_{II\,max} - \Delta K_{II\,min}$,

$\Delta K_I = \Delta K_{III\,max} - \Delta K_{III\,min}$.

The stress intensity factor near the crack tip of the thermal fatigue sample under the cyclic thermal stress is $\Delta K_I = \Delta K_{I\,max} - \Delta K_{I\,min}$, $\Delta K_I = \Delta K_{II\,max} - \Delta K_{II\,min}$ and $\Delta K_I = \Delta K_{III\,max} - \Delta K_{III\,min}$. As suggested by the linear elastic fracture mechanics, the compressive stress does not contribute to the crack propagation [32]. Therefore, upon removal of load, assume neglect thermal deformation, plastic deformation and therefore, all stress become zero when applied pressure is removed i.e. $\Delta K_{I\,min} = \Delta K_{II\,min} = \Delta K_{III\,min} = 0$. The expression in Eq. 3.40 is then used in Paris' law (Eq. 3.41) by substituting ΔK with ΔK_{eff}.

On the other hand, the importance of understanding crack propagation led to a new field of study called fracture mechanics. Paris and Erdogan used the idea of comparing Irwin's stress intensity with the rate of crack propagation per cycle [33]. They developed a relationship between the crack propagation rate per cycle (da/dN) and the stress intensity factor range (ΔK), which is called the Paris' law as shown in Eq. 3.41.

$$\frac{da}{dN} = C\Delta K^m, \quad \textbf{Eq. 3.41}$$

C = $10^{-8.9}$ and m = 4.03 thus are identification parameters of Paris' law [34].

Also, a is the crack length, N is the number of loading cycles, and C and m are the material parameters are obtained by experimentally. Thus, the law identification requires to assess the crack length and SIFs values.

3.7.5 The Analysis of the Crack Propagation Life

As the thermal crack and other fatigue cracks appeared on the brake disc, the Paris' formula could be used to express the crack propagation life according to the fracture mechanics theory[35].

$$N_p = \int_{a_i}^{a_c} \frac{1}{\left(\frac{da}{dN}\right)} da = \int_{a_i}^{a_c} \frac{da}{C(\Delta K)^m}, \quad \textbf{Eq. 3.42}$$

Where: a_i is the initial crack depth; a_c is the critical crack depth; da/dN is the crack growth rate, and ΔK is range of stress intensity factor.

The stress intensity factor (K) was an important index, which reflected the stress field and the strain field of crack tip and was an important parameter to estimate the crack propagation life[36]. Therefore, it was necessary to determine the relationship between crack propagation (da/dN) and the stress intensity factor (K) in the thermal and loading cycle to determine number of failure cycle.

3.8 XFEM Analysis in Abaqus

3.8.1 ABAQUS Software Package

ABAQUS is one of the powerful engineering simulation programs based on the FEM, sold by Dassault Systems as part of their SIMULIA Product Life Cycle Management (PLM) software tools. It is written and maintained by Hibbit, Karlsson and Sorensen, Inc (HKS). It is a highly sophisticated, general purpose finite element program, designed primarily to model the behavior of solids and structures under externally applied loading [37].

The unique features of ABAQUS listed below:

- ABAQUS includes an extensive library of elements that can model virtually any Geometry.
- It allows importing geometry from many different CAD software packages easily.
- Using ABAQUS, we can be able to use different types of material models to simulate the behavior of most typical engineering.
- Designed as a general-purpose simulation tool, ABAQUS can be used to study more than just structural (stress/displacement) problems. It can simulate problems in many diverse areas.
- ABAQUS offers a wide range of capabilities for simulation of linear and nonlinear applications of areas. Problems with multiple components are modeled by associating the geometry defining each component with the appropriate material models and specifying component interactions.

- It can do static as well as dynamic analysis in a good manner.

ABAQUS-standard and ABAQUS-Explicit are two main analysis methods in ABAQUS. ABAQUS-standard is a full purpose analysis module that can solve a variety of problems covering linear and nonlinear problems maintaining the accuracy and the reliability of the results. ABAQUS-Explicit is a special purpose analysis module that uses dynamic finite element formulation, which is applied to deal with the problems of transient and dynamic in nature [38].

ABAQUS-CAE is the total ABAQUS working interface that includes all the options to generate ABAQUS models, to editing models, to submit and monitor jobs for analysis and also a means to review the results.

In this paper , ABAQUS-CAE is important for the preprocessor of different stages of the model creation starting from the edit of Part and assembly, Property, defining the step, Interaction, Load, Mesh and generating the Job from the respective module and postprocessor to extract the results using visualization module. And the post processing is done using ABAQUS/Standard. However, part of dynamic simulation is difficult in my model due to take long time and fail running dynamic explicit as result of distortion of elements.

3.8.2 Brake Disc Geometry Simplification

Since the brake is applied on disc, there is no relative motion of a brake disc on the contact surface of brake disc and pad.

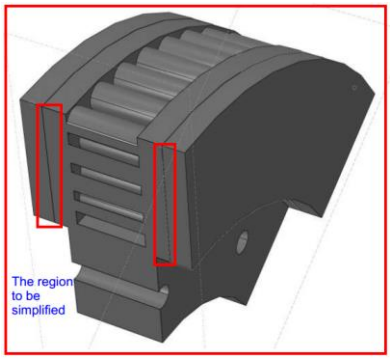

Figure 3-7: The disc region to be simplified

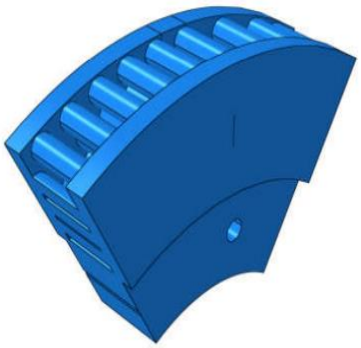

Figure 3-8: Simplified wheel geometry and crack location

For a more simplified analysis, it is better to take a small portion of the disc to apply the loads i.e. both the Mechanical and thermal loads with respect to edge crack on the surface at varying predetermined depth.

3.9 Elastic-Plastic Brake Disc Material Properties

Plastic deformation of material is defined as permanent change in shape or size of a solid body without fracture resulting from the application of sustained stress beyond the elastic limit. Plasticity in metals is usually a consequence of dislocation within the structure.

Plasticity will occur beyond the yield point of the material. Once the load exceeds the yield strength threshold, there is more of a rapid increase in stress than the elastic range, and when the load is removed some amount of the extension still exist which results in permanent deformation [39].

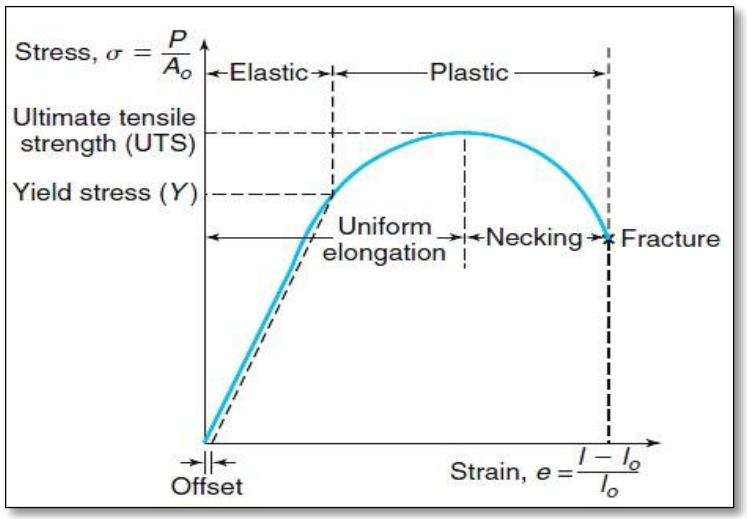

Figure 3-9: A typical stress-strain curve [40]

The ABAQUS software requires that the material be sufficiently defined to provide suitable for those elements with which the material is associated and for all of the analysis procedures through which the model will be run [ABQUS user manual vol.3 Materials]. To perform the elastic-plastic analysis, the elastic mechanical properties are required (which are governed by Hook's Law) because this will provide the stress-strain relationship up to the yield point but additional information is required to ensure the

plastic range is accurately developed. To develop the plastic range in FEA, the Yield and plastic strain need to be manually loaded in to the material properties. If the plasticity data has not been entered into FEA ABAQUS, the stress/strain relationship will continue to be linear. This will not provide an accurate result of stress in the plastic range of deformation.

A power law work hardening model is accepted by most engineering materials such as metals and alloys approximately which is a material constitutive relation and when a metal plastically deformed, dislocations move and also additional dislocations are generated. The modified uniaxial stress-strain (σ-ε) curve of a stress free material can be expressed as [41]:

$$\boldsymbol{\sigma} = E\varepsilon \text{ for } \varepsilon < {}^{\sigma_y}/_{E}\,, \qquad \textbf{Eq. 3.43}$$

$$\boldsymbol{\sigma} = \mathrm{K}\varepsilon^{n} \text{ for } \varepsilon > {}^{\sigma_y}/_{E}\,, \qquad \textbf{Eq. 3.44}$$

Where: E is Elastic modulus, σ_y is yield stress; n is the work hardening exponent and

$\mathrm{K} = \sigma_y(\frac{E}{\sigma_y})^n$ is the work hardening rate. When n is zero the above equation reduces to an elastic-perfectly plastic material. Generally to characterize the elastic-plastic properties of a power-law material, four independent parameters, i.e. elastic modulus, E, yield stress, σ_y, work hardening exponent, n and poison's ratio, ν are needed.

To explain the plastic properties of a material in ABAQUS the power law hardening material model is used, a true stress strain data spreadsheet at first is generated in Excel from the Equation (Eq. 3.43). Then using the equation below (Eq. 3.45), plastic strain (ε_p) is calculated.

$$\varepsilon_p = \varepsilon - \frac{E}{\sigma_y}. \qquad \textbf{Eq. 3.45}$$

3.9.1 Units in ABAQUS Analysis

Since ABAQUS doesn't specify a unit system, the user could use a unit system arbitrarily, as long as they are in consistency in one problem [41]. Therefore, all input data must be specified in consistent units.

Table 3-10: Common consistent units

Quantity	**SI**	**SI(mm)**
Length	M	Mm
Mass	Kg	Tone
Force	N	N
Density	Kg/m^3	$Tone/mm^3$
Time	S	S
Stress	Pa (N/m^2)	Mpa (N/mm^2)
Young's modulus	Pa (N/m^2)	Mpa (N/mm^2)

In this thesis using SI (mm) units that means units for length, force, mass, and young's modulus will be mm, N, Tone, and Mpa, respectively. Young's modulus usually dictates the units of other quantities. Therefore, as per the unit definition the material properties used in ABAQUS are

Table 3-11: Elastic material behavior of the disc material [27][37]

Classification	**Property**	**Value at 25 °C**	**Value at 500 °C**
General	Density	7.25×10^{-9} $Tone/mm^3$	7.25×10^{-9} $Tone/mm^3$
Elastic Region Behavior	Modulus of Elasticity	13,800 N/mm^2	11,8000 N/mm^2
	Poisson's Ratio	0.28	0.28

Density and poisons ratio do not change with changing temperature for metals [https://en.wikipedia.org/wiki/Density]. However, the change is very slight that their effect is negligible.

The Approximate and summarized Material Properties of the disc brake used in crack modeling and stress analysis are listed below [42]:

Temperature (°C)	**Fracture Toughness, K_{IC}**	**Yield Stress, σ_Y**	**Ultimate Strength, σ_{us}**
25	40.2 MPa$\sqrt{m}$	345	388
500	83.7 MPa$\sqrt{m}$	255	265

The plastic region behavior can be represented as:

Table 3-12: Plastic region behavior of the disc material at 25 ^{O}C [43]

No.	Yield stress, ***Mpa***	Plastic strain
1	345	0
2	400	0.0075
3	450	0.016

Table 3-13: Plastic region behavior of the disc material at 500 ^{0}C[43]

No.	Yield stress, ***Mpa***	Plastic strain
1	255	0
2	285	0.0075
3	310	0.019

The Temperature dependent thermal properties are used for the disc brake material to best represent their working condition under high thermal loads during the Analysis. By assuming the increment scheme with respect to temperature, we interpolate the data available in [44][45]**.**

Table 3-14: Temperature dependent thermal properties used in ABAQUS [46][47][44]

Temperature, ^{0}C	Thermal Conductivity, $\times 10^{-3}$ W/m^{0}C	Specific Heat, (J/Kg^{0}C)	Coefficient of Thermal expansion, 10^{-6} /^{0}C
25	54	447	10
100	52.5	492	10.5
200	51.5	561	11
300	50.5	494	11.9
400	49.5	507	12.6
500	48.5	515	13.1
600	47.5	536	13.5
800	45.5	624	14.1
1000	43.5	720	14.7

The XFEM analysis requires material information in the enriched area of crack. The maximum principal (‘*Maxps* Damage’ in ABAQUS) was selected for the damage initiation criteria. The ultimate stress/strength was used as the limiting maximum principal stress. Damage evolution was based on an energy criteria which is equivalent to the strain energy release rate (‘Fracture energy’ on ABAQUS), G_{IC} and a linear softening, maximum degradation a Mode independent.

Fracture energy was estimated using the relationship below [48]:

$$G_{IC} = \frac{K_{IC}^2}{E}. \qquad \textbf{Eq. 3.46}$$

$$= \frac{(40.2)^2 \times 1000}{138000} = 11.71 \text{N/mm}^2 * \text{mm} = 11.71 \text{ kJ at room temperature.}$$

$$= \frac{(83.7)^2 \times 1000}{138000} = 50.766 \text{ N/mm}^2 * \text{mm} = 50.766 \text{ kJ at } 500\ ^{o}\text{C temperature,}$$

where:

G_{IC} is the fracture energy,

K_{IC} is fracture Toughness of the brake disc material

E is young's Modulus of Elasticity.

Crack growth problems require progressive damage, which includes softening and loss of stiffness which can cause severe convergence difficulties. Viscous regularization can be added to analysis ensuring that tangent stiffness matrix is positive definite thereby improving convergence rates. It should be noted that too much stabilization can cause negatively influence of the solution and produce even non-physical results. The value is within the acceptable limit so the Damage stabilization cohesive coefficient is taken as 1E-06 [49].

3.9.2 Convergence Issue Handling

The default time incrementation parameters in ABAQUS are set to achieve some good performance for smooth behavior. However, for discontinuous analysis such as crack growth, the default time integration scheme may result in premature cutbacks and termination. Abaqus/standard abandons iterations and cutbacks the time increment if it finds the residuals are increasing in two consecutive iterations after I_o equilibrium iterations. Another routine check performed is that for logarithmic rate of convergence, based on which the total number of iterations are estimated; if this estimation exceeds I_c, Abaqus/standard reduces the time increment. This check is performed after I_R iterations. The default values of I_o and I_R is 4 and 8 respectively for the continuous domain. For discontinuous domain analysis the values of I_o and I_R are modified as 8 and 10, respectively, cutbacks and reduction in time incrementation are delayed due to it. Also,

the number of attempts for each increment was also increased for their convergence rates.

Therefore, to handle the difficulty of the XFEM convergence issues the minimum time step was set to 1E-20 and the number of increments was increased to 100,000 to prevent premature abortion of the step input. The initial time step for smooth curve simulation a value of 0.5 was used. And beside this the following changes were also made in the step module:

- Step Module → General solution controls → Manager → Edit step → Specify →Time increment→ Discontinuous Analysis→ more I_A=20→ok.
- Step Module → Other →General Solution controls→ Manager →Edit Step → Time Increment → Select Discontinuous Analysis.
- Step Module → Step→ Step Manager→ Edit →Automatic Stabilization → Specify Dissipation Energy fraction→ Accept defaults.

3.9.3 Geometrical Modeling of Disc and Pad Using Solid-work Software

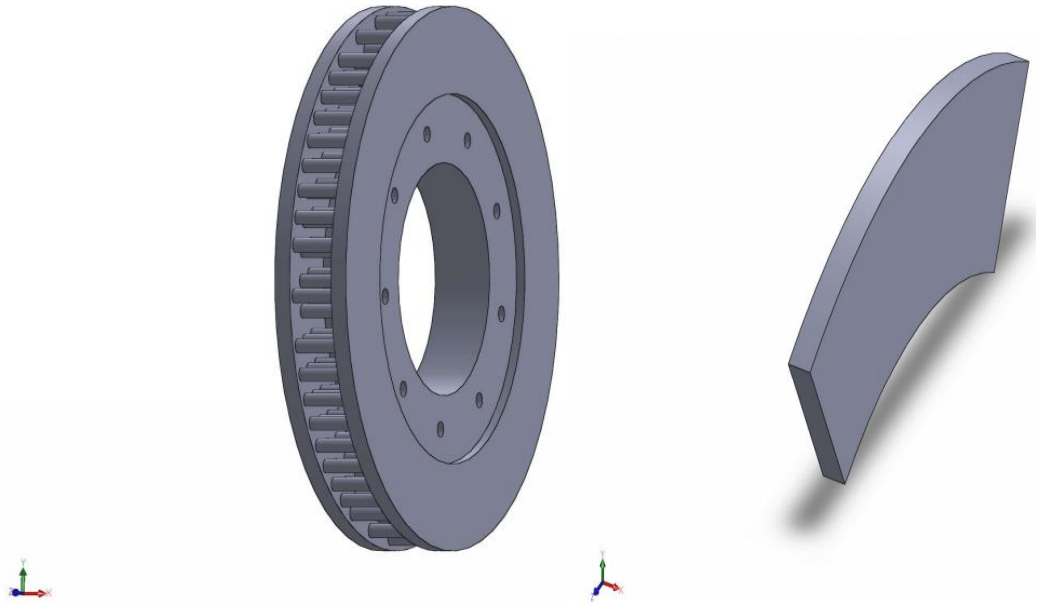

(a) **(b)**

Figure 3-10: (a) 3D model of Disc (b) 3D model of Pad

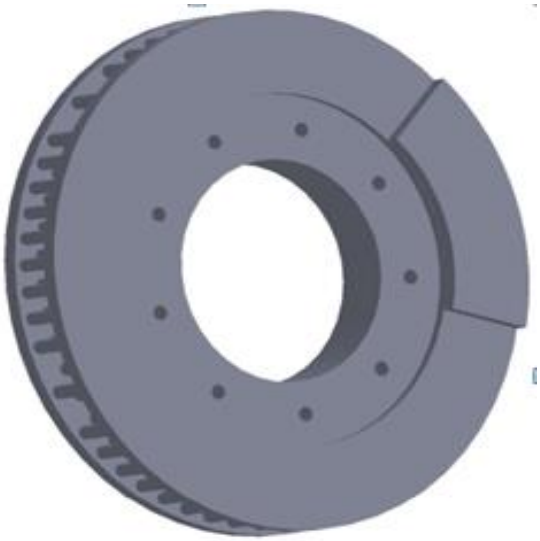

Figure 3-11: Disc and Pad assembling model

3.9.4 Boundary Condition, Loads, and Constraints

The model for this analysis was constructed as a sixth model of disc brake only. To simulate the fixed position of disc, x-z plane faces were constrained boundary condition and to constrain the sixth-model to represent a full model x-y plane was tied to z-direction. The pad pressure load was applied on both surface of disc brake. This load setup is shown in the Figure 3-11.

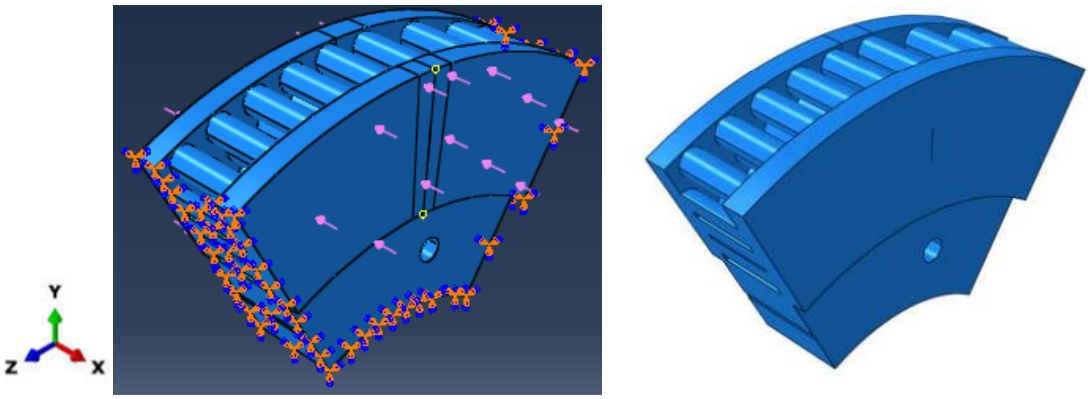

(a) (b)

Figure 3-12:(a) Boundary Conditions and Loads, (b) crack geometry

3.9.5 Meshing of the Disc

Three dimensional (3D) geometrical models of assembled brake disc and pad were built using Solid-work software and then imported into the ANSYS and ABAQUS software for a solid elemental mesh. The mesh process consists of partitioned the disc section into three and applied different element types and edge seeds for each. The elements used for the meshing of the ventilated disc are tetrahedral three-dimensional elements with 10 nodes (C3D10) and then sixth model has totally 319951 nodes and 101988 elements used (Figure 3-13). In this simulation, the meshing was refined around the crack zone of disc. This important because in this zone temperature varies significantly due to this strongly deformed zone, the thermomechanical gradients are very high. That is why the correction taking into account of the contact conditions involves the use of a refined mesh. The figure below shows details of mesh.

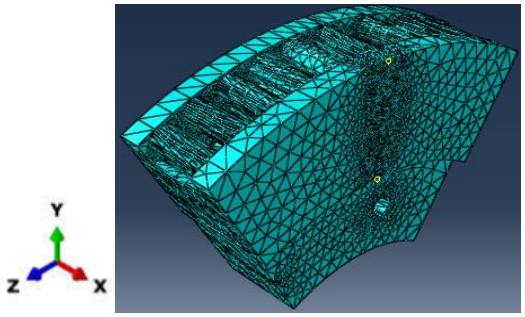

Figure 3-13 Mesh details

CHAPTER 4 XFEM RESULT AND DISCUSION

The analysis done by Abaqus XFEM was performed in two different speeds of train considerations at room 25 ^{o}C and 500 ^{o}C with varying parameters for sensitivity studies. The first analysis was done using a static mechanical load 0.251515 Mpa and 0.254595 Mpa to assess the seriousness of the problem of emergency braking at 40 km/hr and 80 km/hr respectively.

To evaluate the crack tip maximum principal stress and effective stress intensity factor we simulate the disc with crack initial ratio of surface crack depth a_o**:**$2C_o$ = 1**:**4 [19]. Although STATUS XFEM output in the XFEM analysis is red for the stable crack surrounding the crack surface and different color spectrums for the growing cracks and PHILSM and PSILM are the level set values to represent the crack from the normal and tangent directions but, this parameters are not sufficient to understand the crack behavior with increasing length.

4.1 XFEM ABAQUS Result

4.1.1 Effect of Mechanical (Static) Load

The effect of the mechanical load on the crack surface at two different speeds is summarized as shown below.

I. Crack Extension Simulations

Crack Tip Maximum Principal Stress

The first simulation's was conducted in XFEM by increasing the crack length with 4 mm and see the increment of the crack tip principal stress. For example, let's have a look on the five cases of crack lengths i.e. 4, 8, 12, 16, and 20mm. At 4, 8, 12, 16 and 20 mm crack lengths have 8, 17, 17, 16, and 20 crack front node respectively and maximum principal stress based on the number of node and crack length is shown below.

1. Simulation at 40 km/hr in 25 ^{o}C

The stress distributions of the crack tip at room temperature (25 ^{o}C) and normal speed (40 km/hr) disc brake with 4, 8, 12, 16 and 20 mm crack length are shown in the Figure 4-1 to Figure 4-5 respectively. The highest principal stress is lowest at crack size of 8

mm (52 Mpa), see Figure 4-2 and highest at crack size of 16 mm (1.52E4 Mpa), see Figure 4-4.

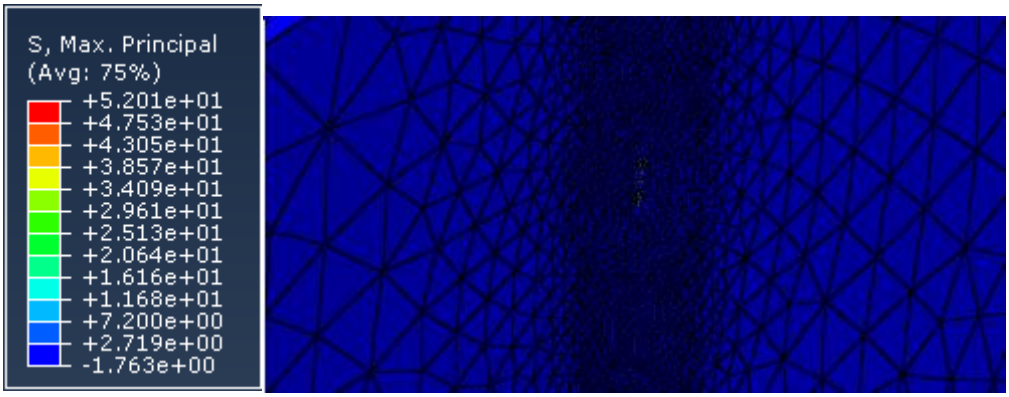

Figure 4-1: Maximum principle stress in Mpa for 4mm crack length

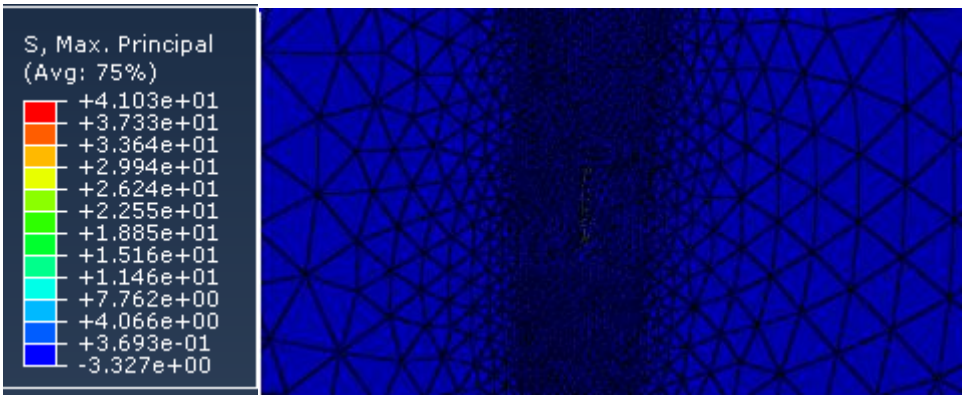

Figure 4-2: Maximum principle stress in Mpa for 8mm crack length

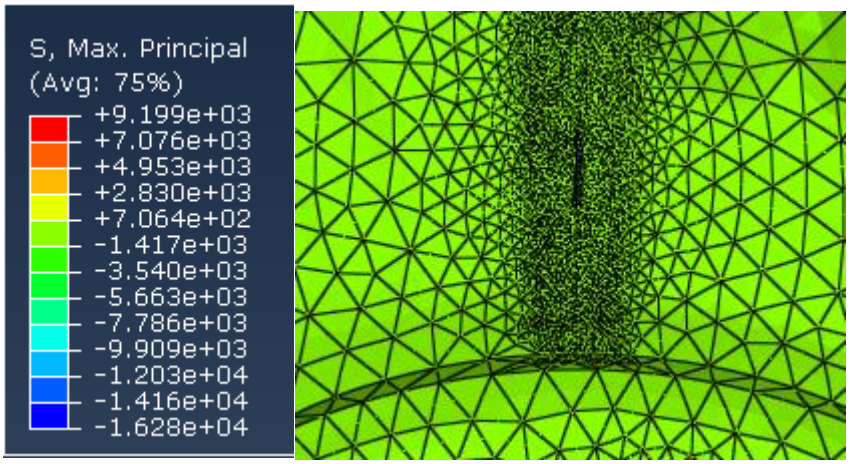

Figure 4-3: Maximum principle stress in Mpa for 12mm crack length

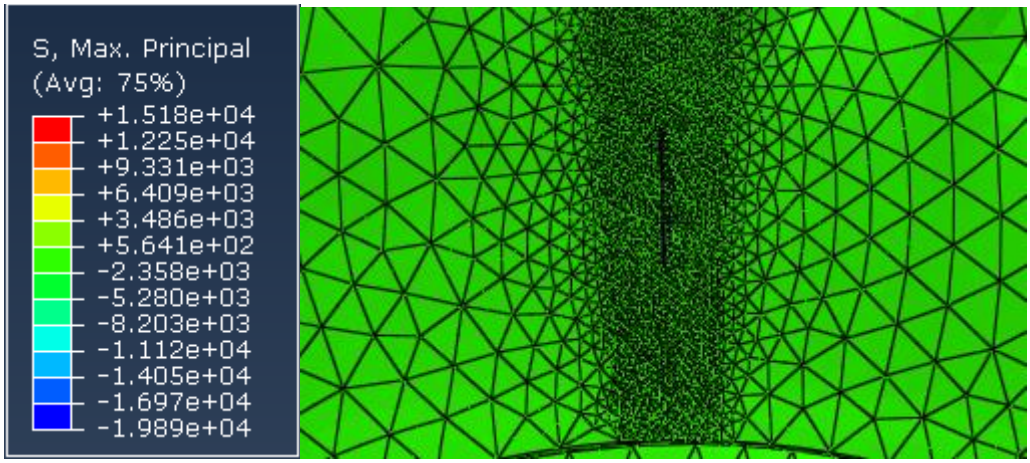

Figure 4-4: Maximum principle stress in Mpa for 16mm crack length

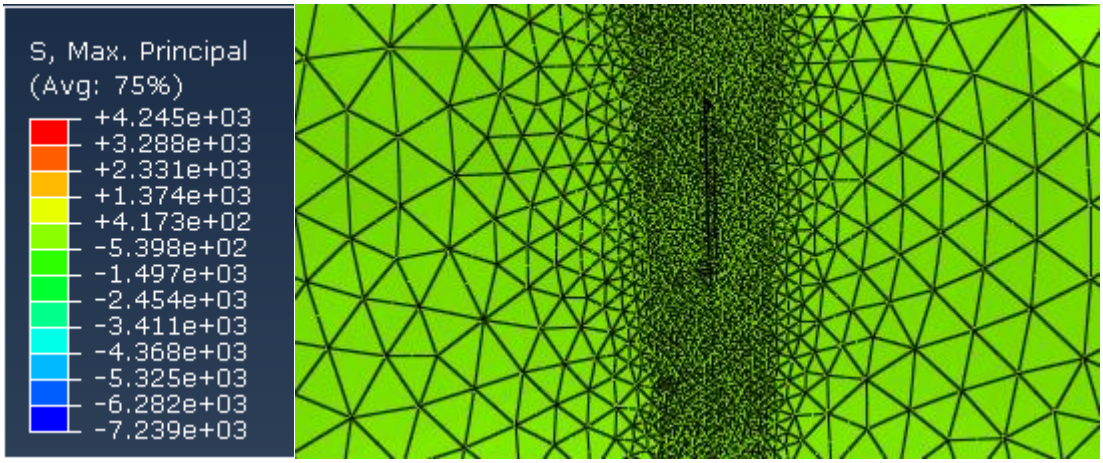

Figure 4-5: Maximum principle stress in Mpa for 20mm crack length

2. Simulation at 80 km/hr in 25 ^{o}C

The stress distributions of the crack tip at room temperature (25 ^{o}C) and at over speed (80 km/hr) disc brake with 4, 8, 12, 16 and 20 mm crack length are shown in the Figure 4-6 to Figure 4-10 respectively. The highest principal stress is lowest at crack size of 8 mm (41.53 Mpa), see Figure 4-7 and highest at crack size of 16 mm (1.52E4 Mpa), see Figure 4-9.

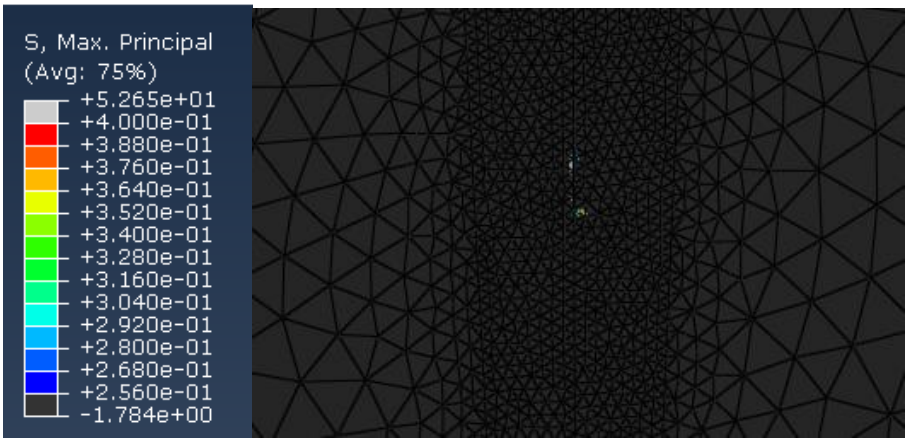

Figure 4-6: Maximum principle stress in Mpa for 4mm crack length

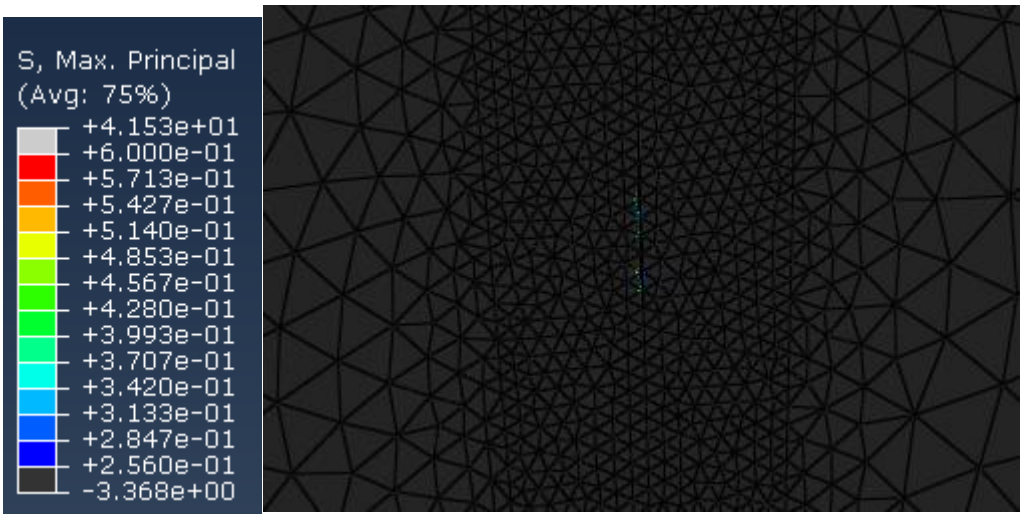

Figure 4-7: Maximum principle stress in Mpa for 8mm crack length

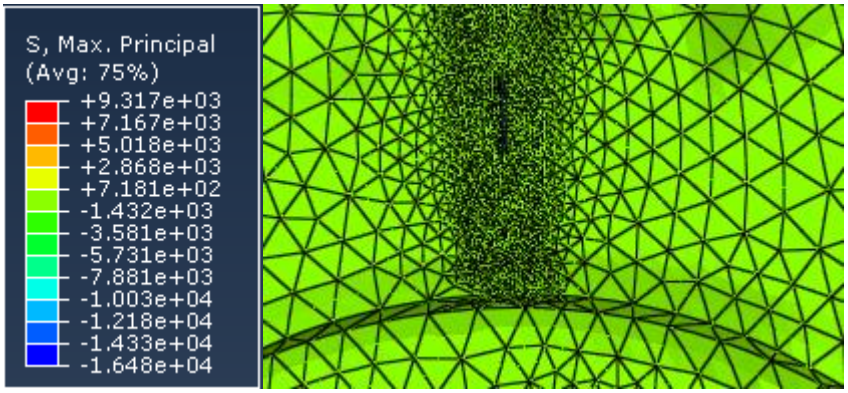

Figure 4-8: Maximum principle stress in Mpa for 12mm crack length

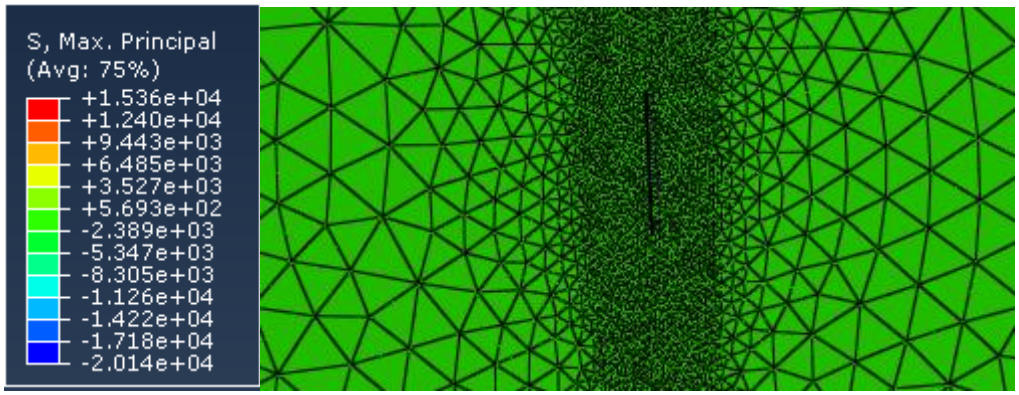

Figure 4-9: Maximum principle stress in Mpa for 16mm crack length

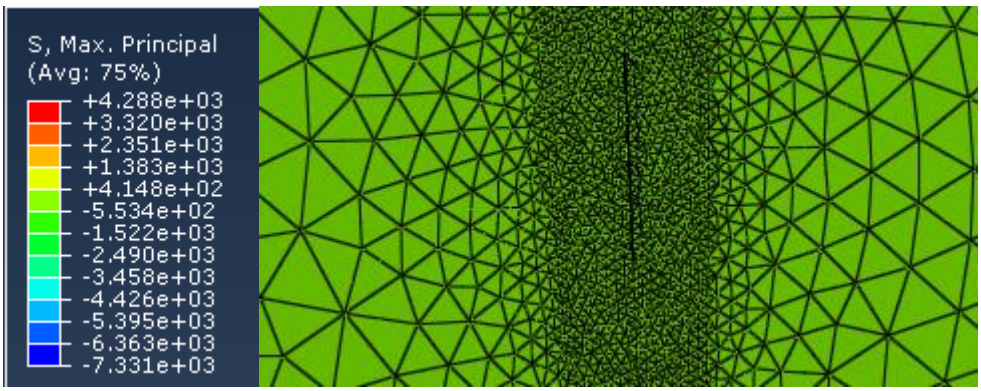

Figure 4-10: Maximum principle stress in Mpa for 20mm crack length

4.1.2 Combined Effect of Frictional Heating Temperature and Mechanical Load

The effect of combined frictional heating temperature and mechanical load on the crack surface at two different speeds is summarized as shown below. At 4, 8, 12, 16 and 20 mm crack lengths have 8, 17, 17, 16, and 20 crack front node respectively.

3. Simulation at 40 km/hr in 500 ^{o}C

The stress distributions of the crack tip at high temperature (500 ^{o}C) and at normal speed (40 km/hr) disc brake with 4, 8, 12, 16 and 20 mm crack length are shown in the Figure 4-11 to Figure 4-15 respectively. The highest principal stress is lowest at crack size of 8 mm (41.03 Mpa), see Figure 4-12 and highest at crack size of 16 mm (1.51E4 Mpa), see Figure 4-14.

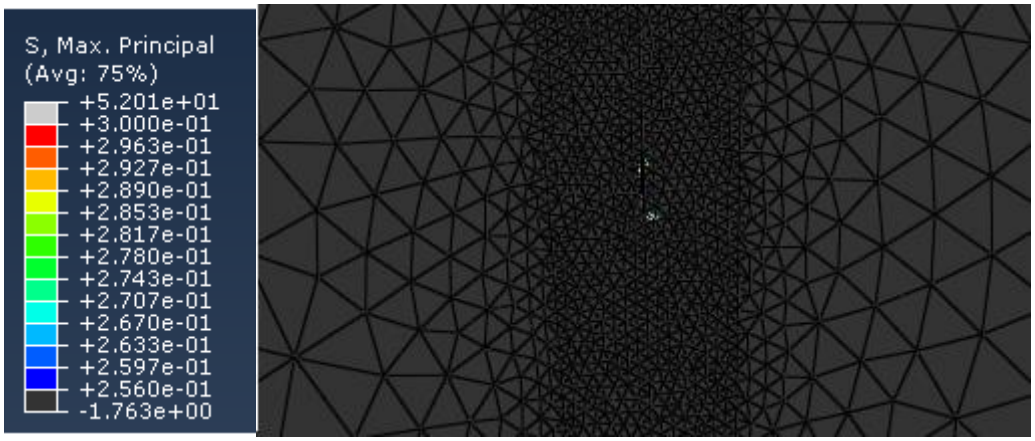

Figure 4-11: Maximum principle stress in Mpa for 4 mm crack length

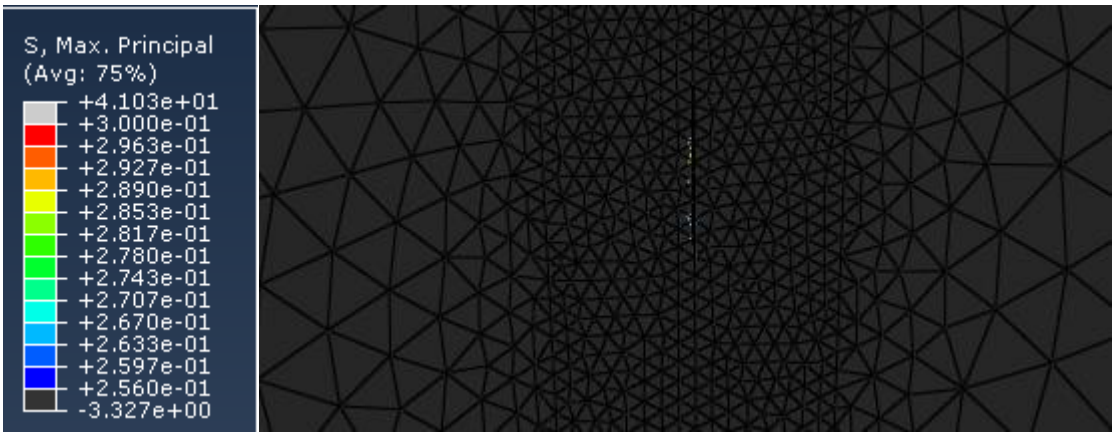

Figure 4-12: Maximum principle stress in Mpa for 8 mm crack length

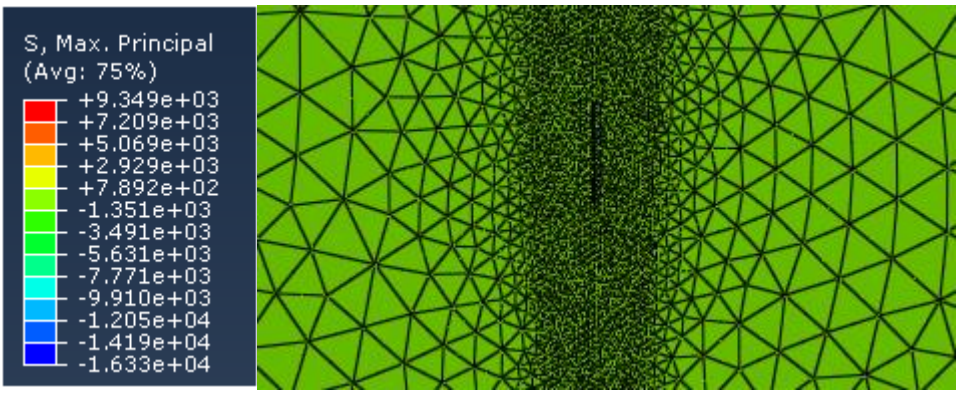

Figure 4-13: **Maximum principle stress in Mpa for 12 mm crack length**

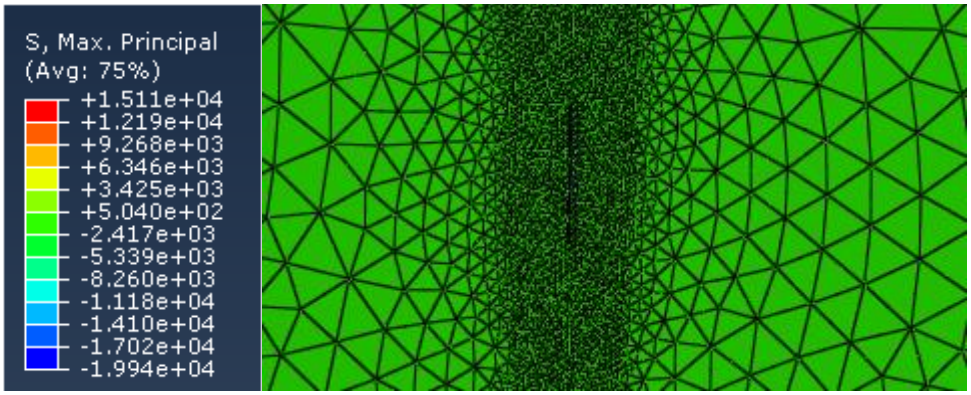

Figure 4-14: Maximum principle stress in Mpa for 16 mm crack length

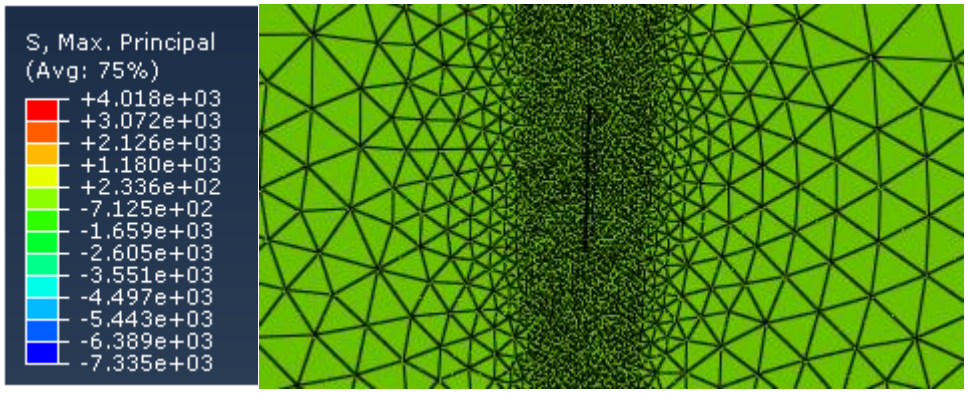

Figure 4-15: Maximum principle stress in Mpa for 20 mm crack length

4. Simulation at 80 km/hr in 500 ^{o}C

The stress distributions of the crack tip at high temperature (500 ^{o}C) and at over speed (40 km/hr) disc brake with 4, 8, 12, 16 and 20 mm crack length are shown in the Figure 4-16 to Figure 4-20 respectively. The highest principal stress is lowest at crack size of 8 mm (41.53 Mpa), see Figure 4-16 and highest at crack size of 16 mm (1.53E4 Mpa), see Figure 4-19.

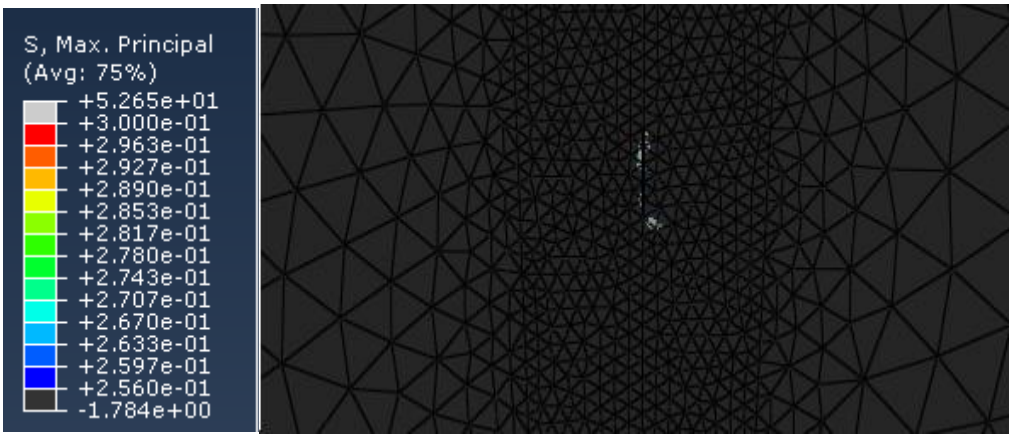

Figure 4-16: Maximum principle stress in Mpa for 4 mm crack length

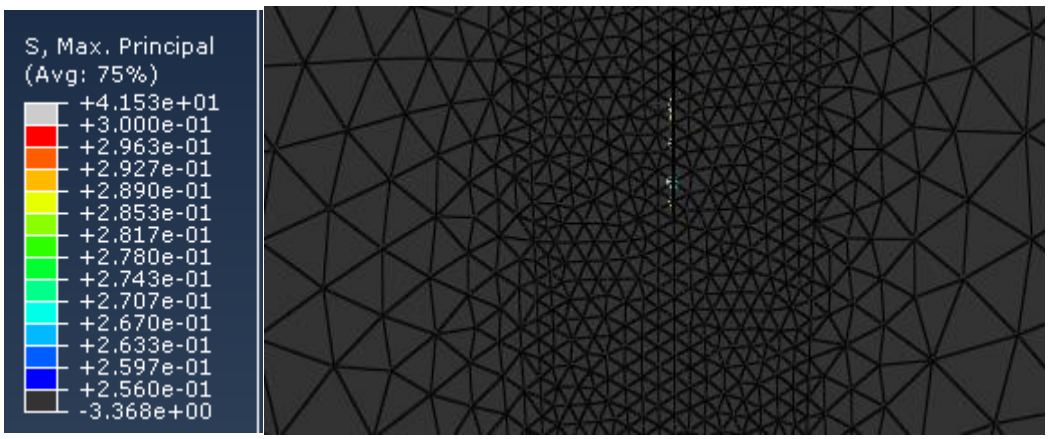

Figure 4-17: Maximum principle stress in Mpa for 8 mm crack length

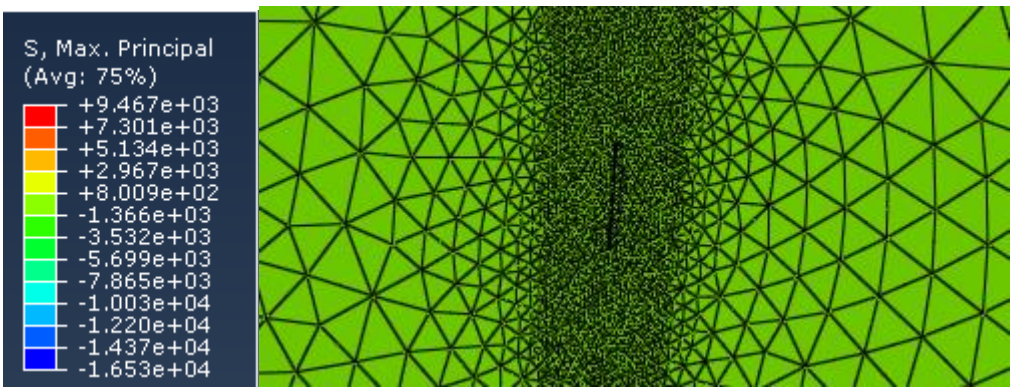

Figure 4-18: Maximum principle stress in Mpa for 12 mm crack length

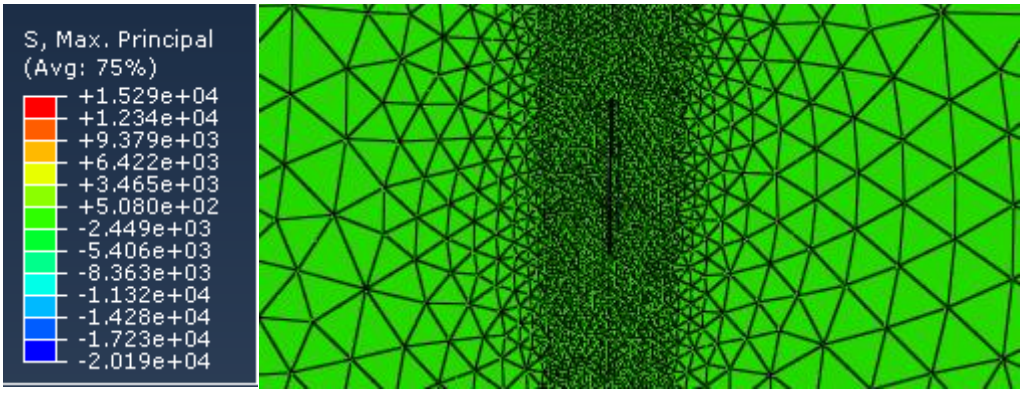

Figure 4-19: Maximum principle stress in Mpa for 16 mm crack length

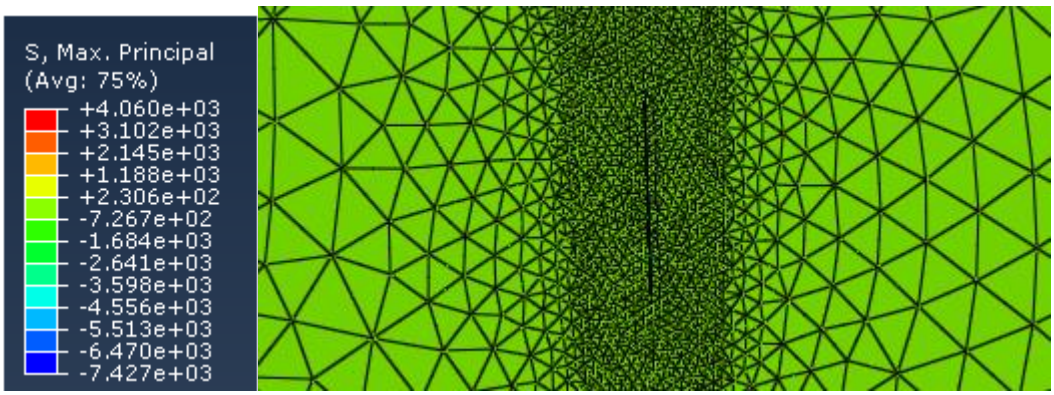

Figure 4-20: Maximum principle stress in Mpa for 20 mm crack length

Therefore, the emergency braking mechanical load and thermo-mechanical load at normal speed and over speed simulation results can be summarized in the table.

The simulation result of crack tip maximum principal stress at normal speed (40 km/hr) in room temperature (25 ^{o}C) and high temperature (500 ^{o}C) and also at over speed (80 km/hr) in room temperature (25 ^{o}C) and high temperature (500 ^{o}C) are obtained, which are shown in Table 4-1. The distribution of effective stress intensity factor at crack front point 4, 8, 12, 16 and 20 mm crack length under normal speed (40 km/hr) in room temperature (25 ^{o}C) and high temperature (500 ^{o}C) and also at over speed (80 km/hr) in room temperature (25 ^{o}C) and high temperature (500 ^{o}C) are summarized in Table 4-2 to Table 4-6 respectively.

Table 4-1: Maximum crack tip principal stress versus crack length

Speed	At 40 km/hr	At 80 km/hr	At 40 km/hr	At 80 km/hr
Temperature	in 25 ^oC		in 500 ^oC	
Crack length (mm)	Maximum crack tip principal stress, Mpa			
4	5.20E+01	5.27E+01	5.20E+01	5.27E+01
8	4.10E+01	4.15E+01	4.10E+01	4.15E+01
12	9.20E+03	9.32E+03	9.35E+03	9.47E+03
16	1.52E+04	1.54E+04	1.51E+04	1.53E+04
20	4.25E+03	4.29E+03	4.02E+03	4.06E+03

Table 4-2: Crack front point effective stress intensity factor versus Crack front point at 4mm crack length

Speed	At 40 km/hr	At 80 km/hr	At 40 km/hr	At 80 km/hr
Temperature	in 25 ^oC		in 500 ^oC	
Crack front Point	Crack Front Point Effective stress intensity factor, $Mpa\sqrt{m}$			
1	0.496913225	0.473252376	0.467539568	0.502958135
2	0.404102097	0.443014939	0.437713504	0.409002124
3	0.244540067	0.24755135	0.244540067	0.24755135
4	0.228378845	0.231181003	0.228378845	0.231181003
5	0.226022517	0.228783467	0.226022517	0.228783467
6	0.25299353	0.256101276	0.25299353	0.256101276
7	0.454129208	0.459731956	0.454129208	0.459731956
8	0.345757921	0.349963641	0.345757921	0.349963641

Table 4-3: Crack front point effective stress intensity factor versus Crack front point at 8mm crack length

Speed	At 40 km/hr	At 80 km/hr	At 40 km/hr	At 80 km/hr
Temperature	in 25 ^oC		in 500 ^oC	
Crack front Point	Crack Front Point Effective stress intensity factor, $Mpa\sqrt{m}$			
1	0.012769484	0.012925768	0.012769484	0.012925768
2	0.012401211	0.012552436	0.012401211	0.012552436
3	0.026294832	0.02661673	0.026294832	0.02661673
4	0.077665273	0.078615897	0.077665273	0.078615897
5	0.258581322	0.261646019	0.258581322	0.261646019
6	0.078979591	0.079947067	0.078979591	0.079947067
7	0.078648424	0.07961098	0.078648424	0.07961098
8	0.093033846	0.094173439	0.093033846	0.094173439
9	0.037742405	0.038203587	0.037742405	0.038203587
10	0.904814808	0.91593691	0.904814808	0.91593691

11	0.241995186	0.245048017	0.241995186	0.245048017
12	0.079806838	0.080783907	0.079806838	0.080783907
13	0.154147032	0.156033855	0.154147032	0.156033855
14	0.228109772	0.230969485	0.228109772	0.230969485
15	0.211467964	0.214002037	0.211467964	0.214002037
16	0.336140042	0.340234387	0.336140042	0.340234387
17	0.226996631	0.229756876	0.226996631	0.229756876

Table 4-4: Crack front point effective stress intensity factor versus Crack front point at 12mm crack length

Speed	At 40 km/hr	At 80 km/hr	At 40 km/hr	At 80 km/hr
Temperature	in 25 ^oC		in 500 ^oC	
Crack front Point	Crack Front Point Effective stress intensity factor, $Mpa\sqrt{m}$			
1	0.811041927	0.787255199	0.777612429	0.820965151
2	0.711276756	0.713061079	0.704444909	0.719893963
3	0.390461621	0.395202207	0.390461621	0.395202207
4	0.113694373	0.115086863	0.113694373	0.115086863
5	0.08304446	0.084061138	0.08304446	0.084061138
6	0.160520882	0.162476655	0.160520882	0.162476655
7	0.228333384	0.231173124	0.228333384	0.231173124
8	0.192034738	0.194335591	0.192034738	0.194335591
9	0.16051386	0.16244146	0.16051386	0.162441278
10	0.127724318	0.129231441	0.127724318	0.129231441
11	0.157647974	0.159582188	0.157647974	0.159582188
12	0.213889181	0.216438083	0.213889181	0.216438083
13	0.157382236	0.15930533	0.157382236	0.15930533
14	0.195487096	0.197929319	0.195487096	0.197929319
15	0.300116316	0.303818891	0.300116316	0.303818891
16	1.038973154	1.059641933	1.046848462	1.051716413
17	0.512720715	0.41087134	0.405923112	0.518993028

Table 4-5: Crack front point effective stress intensity factor versus crack front point at 16mm crack length

Speed	At 40 km/hr	At 80 km/hr	At 40 km/hr	At 80 km/hr
Temperature	in 25 ^oC		in 500 ^oC	
Crack front Point	Crack Front Point Effective stress intensity factor, $Mpa\sqrt{m}$			
1	0.256998002	0.260098406	0.256998002	0.260098406
2	0.228389534	0.231241443	0.228389534	0.231241443
3	0.444180654	0.449658722	0.444180654	0.449658722
4	0.077023034	0.077965471	0.077023034	0.077965471
5	0.070889988	0.071758464	0.070889988	0.071758464
6	2.566525447	2.598480875	2.566525447	2.598480875
7	0.880520831	0.891384645	0.880520831	0.891384645
8	0.298603808	0.302372053	0.298603808	0.302372053

9	0.528671444	0.535108916	0.528671444	0.535108916
10	0.157603616	0.159534316	0.157603616	0.159534316
11	0.4450816	0.450635878	0.4450816	0.450635878
12	0.357781363	0.362178795	0.357781363	0.362178795
13	0.250948719	0.254087823	0.250948719	0.254087823
14	0.115477915	0.116907235	0.115477915	0.116907235
15	0.084999302	0.086041224	0.084999302	0.086041224
16	0.066429788	0.067242964	0.066429788	0.067242964

Table 4-6: Crack front point effective stress intensity factor versus Crack front point at 20mm crack length

Speed	At 40 km/hr	At 80 km/hr	At 40 km/hr	At 80 km/hr
Temperature	in 25 ^{o}C		in 500 ^{o}C	
Crack front Point	Crack Front Point Effective stress intensity factor, $Mpa\sqrt{m}$			
1	1.173765476	1.188105049	1.173765476	1.187818697
2	0.62008609	0.627587394	0.62008609	0.627551429
3	0.311328633	0.315004621	0.311328666	0.315004621
4	0.173406286	0.175528736	0.173406467	0.175528736
5	0.0891703	0.090260665	0.0891703	0.090260665
6	0.167454251	0.169507922	0.167454326	0.169507997
7	0.157102611	0.159007774	0.157102611	0.159007774
8	0.141130083	0.142861764	0.141130083	0.142861764
9	0.113447919	0.114837603	0.113447919	0.114837603
10	0.44376815	0.44915129	0.44376815	0.44915129
11	0.481839448	0.487727865	0.481839448	0.487727865
12	0.177344488	0.179422932	0.177344488	0.179422932
13	0.178513374	0.18073096	0.178513374	0.18073096
14	0.230319437	0.233125298	0.230319437	0.233125298
15	0.262686804	0.265915703	0.262686804	0.265915703
16	0.427681322	0.432989317	0.427681246	0.432989279
17	0.545199515	0.551909138	0.54519943	0.551909053
18	0.482766989	0.488703553	0.48276698	0.488703544
19	0.253728943	0.256847432	0.253728841	0.256847432
20	0.166431712	0.168435951	0.166431712	0.168435951

The effective stress intensity factor at crack length of 4, 8, 12, 16 and 20 mm under normal speed (40 km/hr) in room temperature (25 ^{o}C) and high temperature (500 ^{o}C) and also at over speed (80 km/hr) in room temperature (25 ^{o}C) and high temperature (500 ^{o}C) are summarized in Table 4-7.

After crack generating, mechanical and thermos-mechanical crack propagation rate (da/dN) are obtained by Eq. 3.41 and simulation result under normal speed (40 km/hr) in room temperature (25 ^{o}C) and high temperature (500 ^{o}C) and also at over speed (80

km/hr) in room temperature (25 ^{o}C) and high temperature (500 ^{o}C) are summarized in Table 4-8. The numbers of failure cycles are determined by Eq. 3.42 under normal speed (40 km/hr) in room temperature (25 ^{o}C) and high temperature (500 ^{o}C) and also at over speed (80 km/hr) in room temperature (25 ^{o}C) and high temperature (500 ^{o}C) are shown in Table 4-9.

Table 4-7: Effective stress intensity factor versus crack extension

Speed	At 40 km/hr	At 80 km/hr	At 40 km/hr	At 80 km/hr
Temperature	in 25 ^{o}C		in 500 ^{o}C	
Crack Length, mm	Crack length Effective stress intensity factor, $Mpa\sqrt{m}$			
4	0.227200681	0.229982235	0.227200681	0.229982235
8	0.037742405	0.038203587	0.037742405	0.038203587
12	0.16051386	0.16244146	0.16051386	0.162441278
16	0.413637626	0.418740485	0.413637626	0.418740485
20	0.462803799	0.468439578	0.462803799	0.468439578

Table 4-8: Crack propagation rate ($\boldsymbol{da/dN}$) versus crack length

Speed	At 40 km/hr	At 80 km/hr	At 40 km/hr	At 80 km/hr
Temperature	in 25 ^{o}C		in 500 ^{o}C	
Crack Length, mm	Crack propagation rate (da/dN), mm/ cycle			
4	3.21145E-12	3.37286E-12	3.21145E-12	3.37286E-12
8	2.31736E-15	2.43361E-15	2.31736E-15	2.43361E-15
12	7.91746E-13	8.30767E-13	7.91746E-13	8.30763E-13
16	3.59211E-11	3.77406E-11	3.59211E-11	3.77406E-11
20	5.64833E-11	5.93068E-11	5.64833E-11	5.93068E-11

Table 4-9: Number of failure cycle versus crack length

Speed	At 40 km/hr	At 80 km/hr	At 40 km/hr	At 80 km/hr
Temperature	in 25 ^{o}C		in 500 ^{o}C	
Crack Length, mm	Number of emergency braking times, cycles			
4	1.24554E+12	1.18594E+12	1.24554E+12	1.18594E+12
8	3.4522E+15	3.2873E+15	3.4522E+15	3.2873E+15
12	1.51564E+13	1.44445E+13	1.51564E+13	1.44446E+13
16	3.34066E+11	3.1796E+11	3.34066E+11	3.1796E+11
20	3.54087E+11	3.37229E+11	3.54087E+11	3.37229E+11

4.2 The Curve of the Maximum Principle Stress in Crack Length

The Extended Finite Element Method is used to simulate thermos-mechanical stress response. The stress distributions of the crack tip at room temperature (25 ^{o}C) and high temperature (500 ^{o}C) with normal speed (40 km/hr) and over speed (80 km/hr) are shown in Figure 4-1 to Figure 4-20.

The effect of speed and temperature are on crack tip stress has its own contribution as shown put clearly in Table 4-1. Totally when speed and temperature increases the MAXPS also increase. The result shows that the maximum crack tip principal stress of the disc will increases until 16 mm crack extension and also after 16 mm crack grows decrease maximum principal stress this indicates that crack extension easily propagates after 16mm crack as shown in Figure 4-21. However, the maximum crack tip principal stress at 132 mm crack length is 1424.3 Mpa [19]. The result of this research is a little bite different due to material type, speed and crack length.

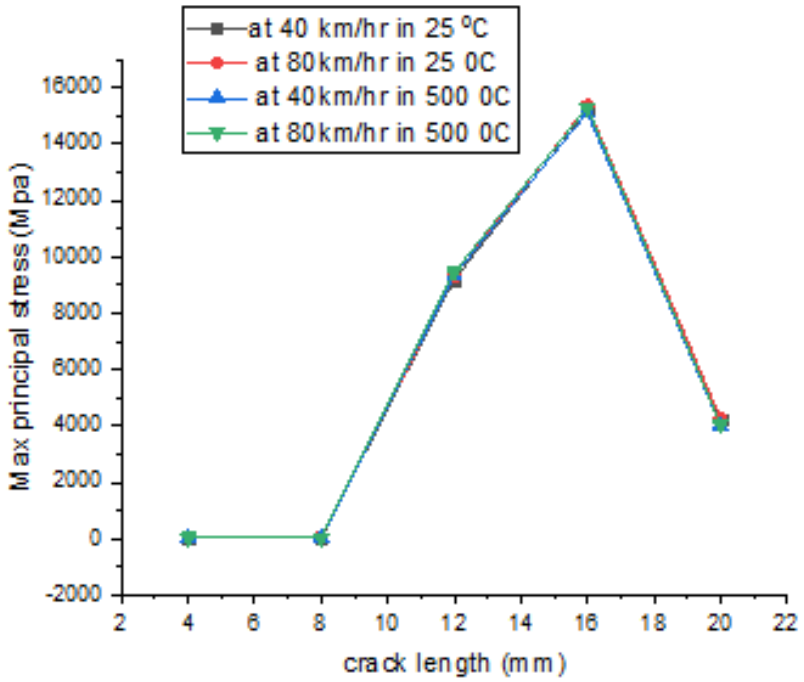

Figure 4-21: Crack tip maximum principal stress versus Crack length

4.3 The Curve of Stress Intensity Factor at Crack front Point

The thermos-mechanical effect of effective stress intensity factor at crack tip front point, in 4, 8, 12, 16 and 20 mm crack length are clearly shown in the Figure 4-22 to Figure

4-26 below respectively. The result shows that at over speed and high temperature the stress intensity factor is greater than those obtained at low speed and low temperature (Table 4-2). Thus results indicate that speed and temperatures have its own contribution of the crack. The middle crack front point shows the average of SIFs as shown in Figure 4-22 i.e. the combined effective stress intensity factor near the crack tip of the thermos-mechanical fatigue crack are determined by Eq. 3.40 . looking on Figures 4-22, 4-23, 4-24, 4-25 and 4-26 the highest stress intensity factor is lowest at crack size of 4 mm (0.5 Mpa) sqr(m), see Figure 4-22 and highest at crack size of 16 mm (2.5 $Mpa\ sqr(m)$, see Figure 4-25). The reason that the highest effective stress intensity factor at crack size of 16 mm is higher than that of crack size of 20 mm (see Figure 4-27) is because as the crack reaches the total rupture, the stresses will reduce. This also is in correlation to the known stress-strain curve.

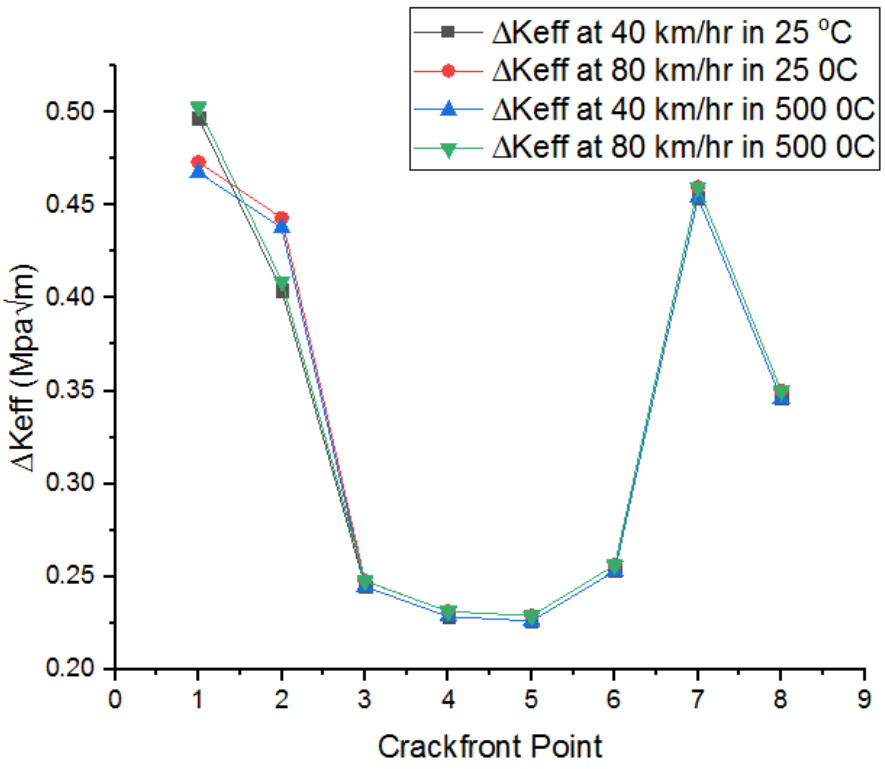

Figure 4-22: Stress intensity factor versus Crack front point at 4 mm crack length

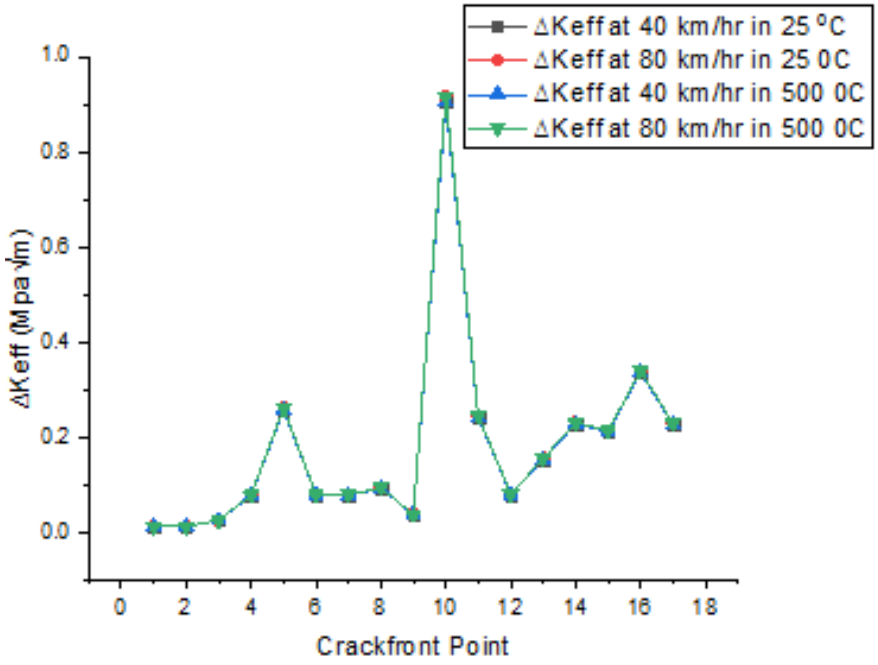

Figure 4-23: Stress intensity factor versus Crack front point at 8 mm crack length

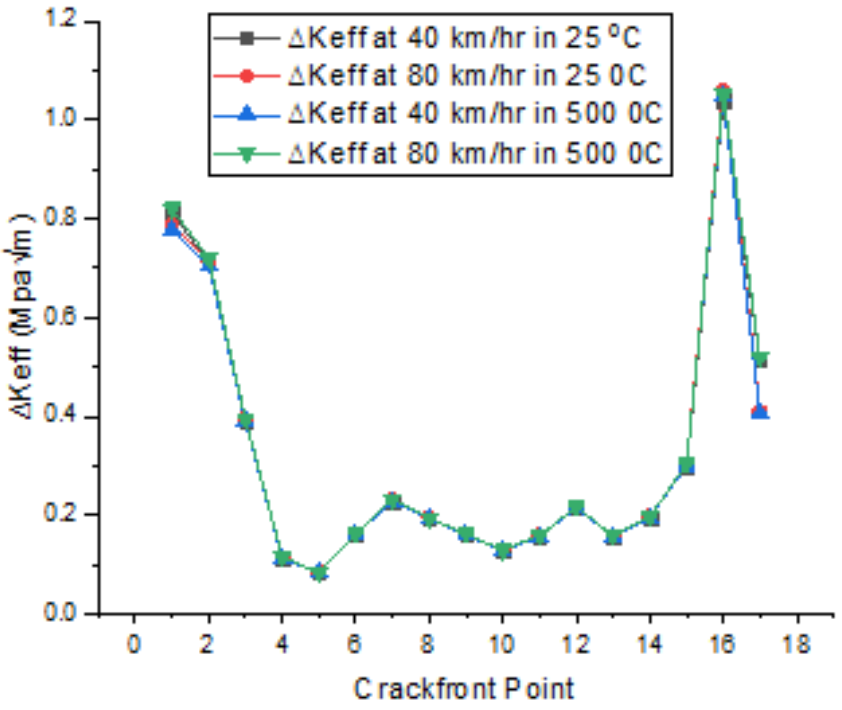

Figure 4-24: Stress intensity factor versus Crack front point at 12 mm crack length

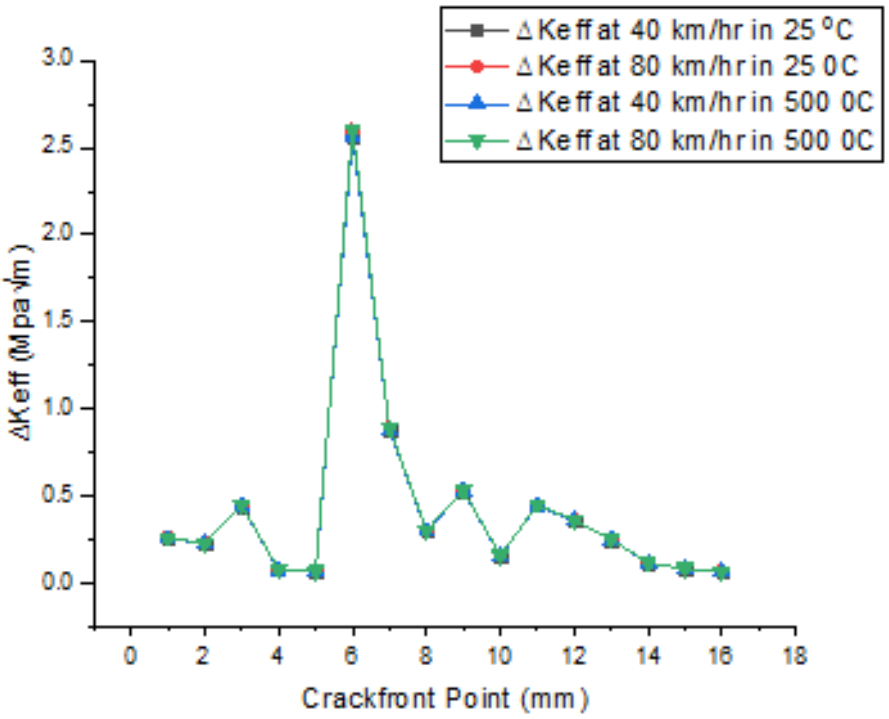

Figure 4-25: Stress intensity factor versus Crack front point at 16 mm crack length

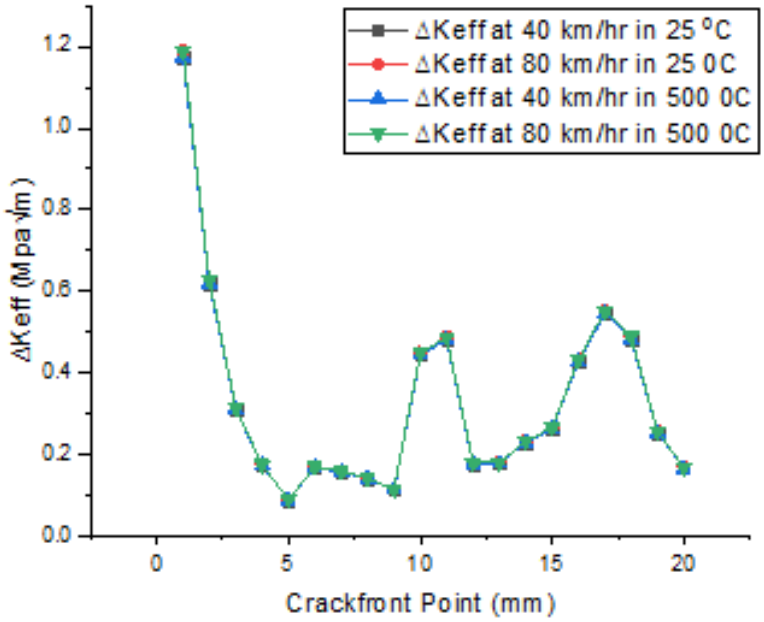

Figure 4-26: Stress intensity factor versus Crack front point at 20 mm crack length

4.4 The Curve of Stress Intensity Factor in Crack Extension

According to the results of thermos-mechanical fatigue crack propagation simulation, five crack lengths (4, 8, 12, 16 and 20 mm) are chosen to calculate the cyclic load stress and the corresponding range of the stress intensity factor range can be obtained as shown in Figure 4-27. The SIFs at 4 mm length are greater than 8 mm thus indicates that before crack formation needs more SIFs and after 8 mm increasing up to 16 mm and also after 16 mm the increment is small compared.

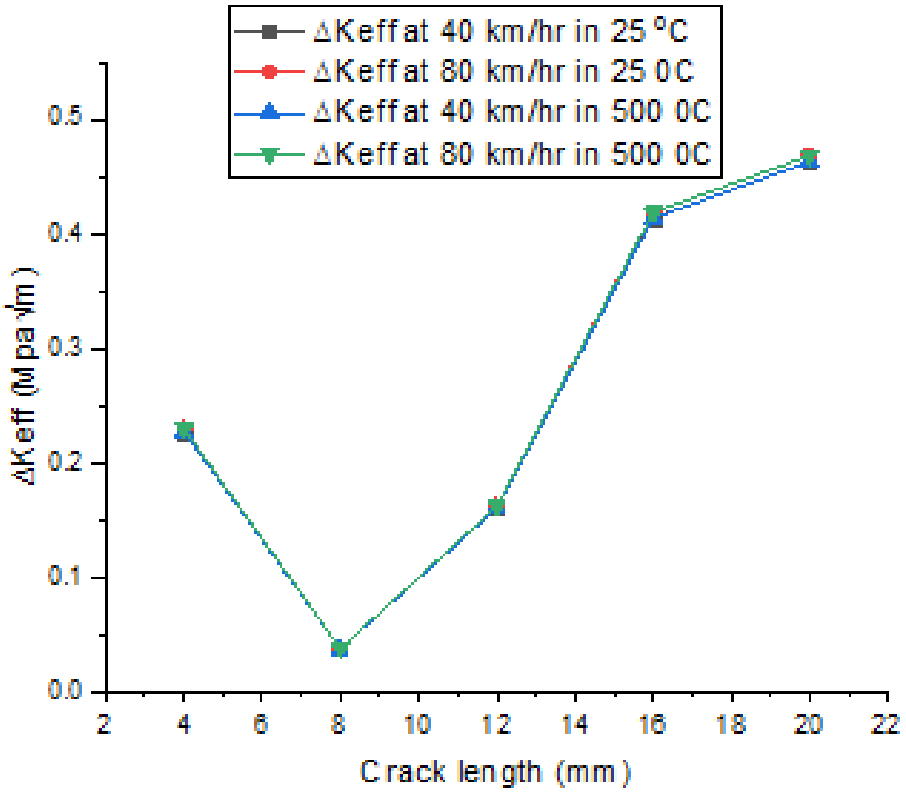

Figure 4-27: Effective stress intensity factor versus Crack length

4.1.3 Determination of the Parameters of the Crack Propagation Curve

The crack propagation rate (da/dN) obtained by Paris law in Eq. 3.41 and the range of the stress intensity factor (ΔK_i) determined by the Extended finite element method are used to obtain the corresponding. The curve shown in Figure 4-28 shows that the propagation rate is increasing after 12 mm length and also both speed and temperature have a great contribution to accelerate propagation rate.

The number of failure cycle's disc brake was determined by Eq. 3.42 as shown in Figure 4-29 at 4 mm has small cycles to occur failure on the disc surface and at 8 mm has the highest cycles to occur failure. After 8 mm the cycles decrease up to 12 mm crack length and also slight difference after 12 mm. This indicates that after 8 mm the disc the failure is easily occur within short period of time (cycle).

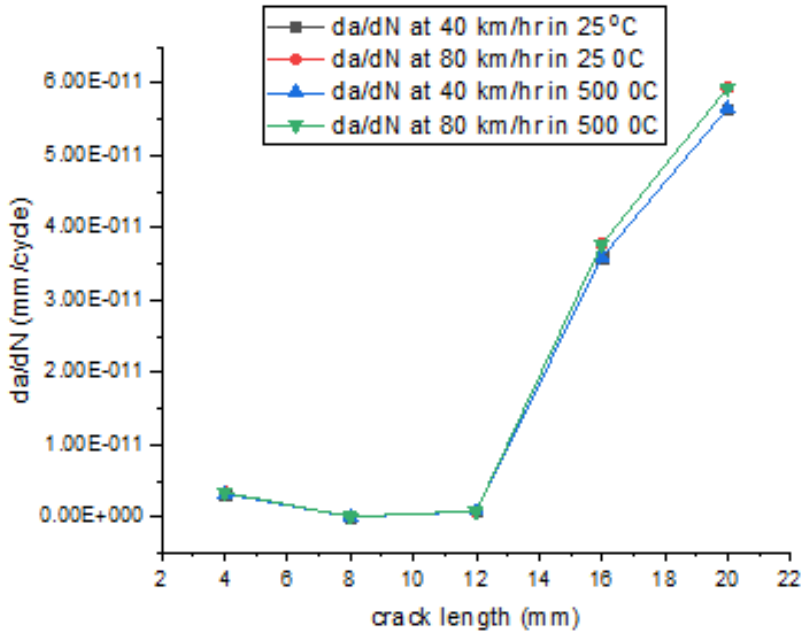

Figure 4-28: Crack propagation rate versus crack length

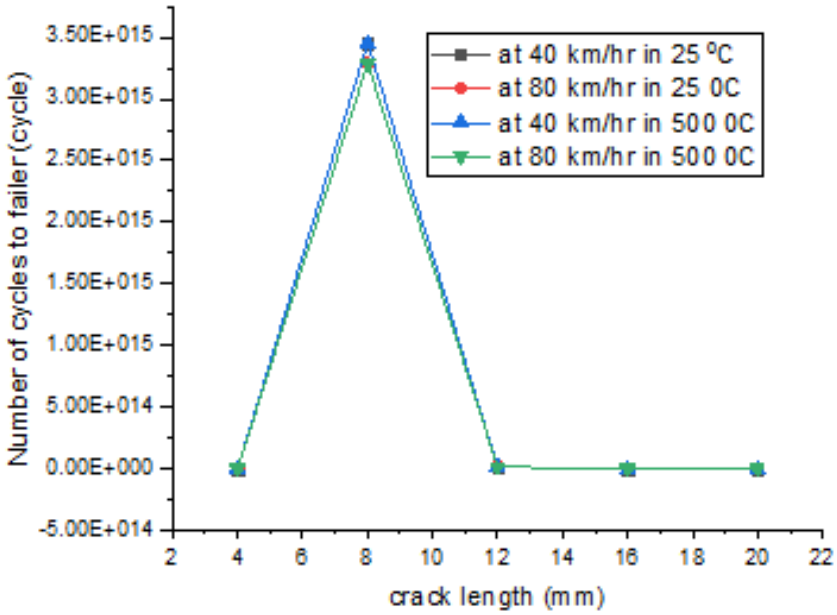

Figure 4-29: Number of cycles to failure versus crack length

4.5 Discussions

In the Abaqus XFEM, AALRT train disc brake model under combined load of Mechanical and Temperature at the surface with different crack lengths at normal speed and over speed emergency braking in downhill gradient were simulated. It is of vital importance to note that current work on the mechanical and thermo-mechanical fatigue crack propagation analysis of grey cast iron disc at braking speed of 40 km/hr and 80 km/hr as shown in Figure 4-28. The range of stress intensity factor (ΔK_i) determined by the extended finite element method as shown Table 4-7 and The crack propagation rate (da/dN) obtained by Paris' equation (Eq. 3.41) are used to obtain the corresponding points as shown in Figure 4-28 and also the number of failure cycle is determined by Eq. 3.42, the number of emergency braking cycle times to failure of disc brake at different crack length was done as shown in Figure 4-29.

From the literature mostly the relationship between number of failure cycles and crack length has directly proportional relation [20][19] but from my research at 8 mm crack length as shown in Figure 4-29 has highest failure cycle among 4, 12, 16 and 20 mm crack length, this result is based on maximum crack tip stress and crack propagation rate as shown in Figure 4-21 and Figure 4-28 respectively. It indicates after 8 mm crack length needs a small number emergency braking to occur crack failure and also the difference of stress intensity factor between literature and this thesis is based on material type, speed and crack length.

Besides, it appears that mechanical loading of friction effect and contact pressure can also play a very important role accelerating crack propagation rate, the present work focuses on a single permitted fatigue crack. Actually, there are tremendous amount of parallel "long'' and "short'' cracks simultaneously appear and evolve at outer surface and insides of the braking disc [19]**.** The interaction effect and proper simplification of multiple separate cracks are a very challengeable task.

CHAPTER 5 CONCLUSION AND RECOMMENDATION

5.1 Conclusion

In this thesis work, the fatigue crack propagation analysis of disc brake under normal and over speed and also with acceptable load was done using Extended Finite Element Method (XFEM).

The finite element gives a good prediction in terms of crack shape evolution, and hot spots of crack growth. In addition, it is much less time consuming.

This thesis goes through 3D crack growth simulation of disc brake radially on the frictional surface by applying static mechanical load and thermos-mechanical load on it for the crack propagation and stress distribution with stress intensity factor schemes using a method of Extended Finite Element Method (XFEM). The results indicate that after 14mm crack length the crack easily propagate and during over speed the stress concentration is large with compared normal speed. The simulation shows that the influence of speed and temperature when temperature and speed increase with crack propagation rate.

This study gives an exploratory investigation on the predicted methodology and the results of thermos-mechanical fatigue crack growth under consecutive emergency braking for normal and over speed of AALRT brake disc.

The present study can provide a useful tool for disc brake maintenance purpose based on propagation rate and failure cycle. It foretells how fast the crack will propagate once after detecting it and measuring its size. This study also provides a method to estimate the remaining fatigue life of present crack in brake disc. The maximum temperature, stress and total deformation of the result could be with in the design limit, but moving a vehicle at a high speed and load increasing could increase crack propagation of the disc brake.

5.2 Recommendations and Future work

During the overall evolution of this study, some research gaps in the area of modeling cracks for railway applications are observed. Some of the gaps that should be filled are:

- Modeling of brake disc cracks under "fully coupled Mechanical and Thermal stress'' (i.e. the thermal load is fully dependent on mechanical load on the cracked system) of the mating surface i.e. disc and pad in XFEM. As per the future Abaqus and LS-Dyna XFEM capabilities.
- Experimental validation of the thermal heat flux effect on the subsurface and surface defects of a railway disc brake.
- Development of new material of disc brake that resist thermos-mechanical effect better than the present material.
- Experimental studies of effect of temperature on fatigue properties of disc brake materials.
- Effect of braking energy on residual stresses in disc brake.
- Determination of crack initiation sites.

REFERENCES

[1] Zwierczyk PT. Thermal and stress analysis of a railway wheel-rail rolling-sliding contact 2015.

[2] A. Stephens,‟ Aerodynamic Cooling of Automotive Disc Brakes,” School of Aerospace, Mechanical & Manufacturing Engineering RMIT University, March 2006.

[3] Jenkins P, Deal D, Cuthbertson T, Morton J, Smith A, Hoy D, et al. System for monitoring vehicle efficiency and vehicle and driver perfomance 2001.

[4] Duranton C. Fatigue analysis of two wheel-mounted brake disc designs 2015.

[5] Grieve D.G, Barton D. c, Crolla D. A, Buckingham J. T (1998), Design of a light weight automobile brake disc using finite element and Taguchi techniques, proc. Instn. Mech. Engrs.Vol. 212,No 4, 245-254.

[6] Kajela Temesgen, „Thermal Stress Analysis of Disc Brake Rotor by Finite Element Method‟‟,Addis Ababa University institute of Technology School of Mechanical and Industrial Engineering, Ethiopia, 2014.

[7] Tsegaye Feleke,” Rail braking vehicle system (MEng 6403)‟‟‟‟,Addis Ababa University,Ethiopia.

[8] Libo Tango and Guoslun Wang ―Simulation Analysis of Train Brake Disc Brake Temperature Field‖, 2012.

[9] Hwang, Pyung and Wu X. Investigation of temperature and thermal stress in ventilated disc brake based on 3D thermo-mechanical coupling model. J Mech Sci Technol 2010;24:81–4.

[10] T.L. Anderson, Fracture Mechanics: Fundamentals and Application 3rd Edition, Taylor and Francis group, 2005.

[11] Majid Mirzaei. Fracture Mechanics: Theory and Applications-Lecture notes, TM university 2014.

[12] Samrawit Addis, Analysis of crack propagation in rotating composite Disc, MSc. Thesis, Addis Ababa university, 2010.

[13] N.K. Simha, F.D. Fischer, G.X. Shan, C.R.Shan, C.R.Chen, O.Kolednik, Jintegral and crack driving force in elastic-plastic materials, Journal of Fracture Mechanics and Physics of solids 56(2008) 2876-2895.

[14] Mohamed RehanKarim―Degree of Train Overloading and its Implication on Road Safetyin Developing Countries‖2012.

[15] Ali Belhocine and MostefaBouchetara, Thermal- mechanical coupled analysis of a brake disc rotor, University of Sciences and the Technology of Oran, L.P 1505 El -MNAOUER, USTO 31000 ORAN (Algeria).

[16] Zaid, M.A., Radzai, M.S., Ahmed, R., Ridzuan, M.M., nurfaizey, A.H., and Afanizam/ M.M.R., ―An Investigation of Disc Brake Rotor by Finite Element‖ July-December 2009.

[17] Eticha AK. Analysis of the Performance of Disc Brake System of Addis Ababa Light Rail Transit Using Temperature and Coefficient of Friction as a Parameter 2016;4:205–11. doi:10.11648/j.ijmea.20160406.11.

[18] Li Z, Han J, Yang Z, Pan L. The effect of braking energy on the fatigue crack propagation in railway brake discs. Eng Fail Anal 2014;44:272–84.

[19] S.C. Wu ⇑, S.Q. Zhang, Z.W. Xu, State Key Lab. of Traction Power, Southwest Jiaotong University, Chengdu 610031 PC. Thermal crack growth-based fatigue life prediction due to braking for a high-speed railway brake disc 2016;359–369.

[20] Yang G, Yang Y. Investigation on the Thermal Fatigue Life Evaluation Method of Railway Brake Disc with New Material. Teh Vjesn 2018;25:1095–102.

[21] Technical Specifications of Vehicles, South-north Line and East-west Line (Phase I) Light Rail EPC Project of Addis Ababa, 2013, Ethiopia.

[22] Tompkin JB. Development of the Disc Brake with Particular Reference to British Railways Application. J Inst Locomot Eng 1969;59:84–129.

[23] Saiz CB, Ingrassia T, Nigrelli V, Ricotta V. Thermal stress analysis of different full and ventilated disc brakes. Frat Ed Integrita Strutt 2015;9.

[24] Milošević MS, Stamenković DS, Milojević AP, Tomić M. Modeling thermal effects in braking systems of railway vehicles. Therm Sci 2012;16:515–26.

[25] Material property of gray cast iron, ANSYS software14.5.

[26] Tompkin, J.B. KI of LE. Development of the Disc Brakes with Particular Reference to British Railway Application, 1969:84–129.

[27] Thermal analysis of both ventilated and full disc brake rotors with frictional heat generation 2014:5–24.

[28] Miloš S. Milošević, Dušan S. Stamenković, Andrija P. Milojević, and Miša M. TOMIĆ,modeling thermal effects in braking systems of railway trains, Faculty of Mechanical Engineering, University of Niš, Niš, Serbia.

[29] Miloš S. Milošević, Dušan S. Stamenković, Andrija P. Milojević, and Miša M. TOMIĆ,modeling thermal effects in braking systems of railway trains, Faculty of Mechanical Engineering, University of Niš, Niš, Serbia.

[30] Gigan GL, Vernersson T, Lundén R, Skoglund P. Disc brakes for heavy vehicles an experimental study of temperatures and cracks. Proc IMechE Part D: J Automob Eng 2014(Spcial Issue):1–24.

[31] Tanaka K. Fatigue crack propagation from a crack inclined to the cyclic tensile axis. Eng Fract Mech 1974;6:493–507.

[32] Donzella G, Scepi M, Solazzi L, Trombini F. The effect of block braking on the residual stress state of a solid railway wheel. Proc Inst Mech Eng Part F J Rail Rapid Transit 1998;212:145–58.

[33] P.C. Paris and F. Erdogan. (1963). “A critical analysis of crack propagation laws,” J. Basic Eng., 85(4), 528-534.

[34] Jerome Hosdez, J-F Witz, C. Martel, N. Limodin, D. Najjar, E. Charkaluk P, Osmond FS. Fatigue crack growth law identification by Digital Image Correlation

and electrical potential method for ductile cast iron 2017.

[35] Gao, Q. (1986). Engineering fracture mechanics. Chong Qing, CQ: Chongqing University Press.

[36] Cheng, J. & Zhao, S. S. (2006). Fracture mechanics. Bei Jing, BJ: Science Press.

[37] Gaël Le Gigan, Magnus Ekh, Tore Vernersson R. Modeling of Grey Cast Iron for application to brake disc for heavy vehicles 2017.

[38] Dessault systems, Abaqus Manual, 2012.

[39] Hsu C-H, Lee S-C, Shy Y-H, Feng H-P. The effect of testing temperature on fracture toughness of austempered ductile iron. Metall Mater Trans A 2001;32:295–303.

[40] Richard G.Budynas JKN. Mechanical Engineering design (9th Edition), Mc-Graw Hill companies, New York, 2011.

[41] Kurapati SNVRK. Elastic-plastic indentation deformation in Homogenous and Layered materials: Finite Element Analysis, University of Kentuky Master's Thesis, 2008.

[42] CHENG-HSUN HSU, SHEN-CHIH LEE, HUI-PING FENG and Y-HS. The Effect of Testing Temperature on Fracture Toughness of Austempered Ductile Iron n.d.;VOLUME 32A:295–305.

[43] Márquez P. Evaluation of Material Parameters of Cast Iron 2015.

[44] Caprioli S. Short rolling contact fatigue and thermal cracks under frictional rolling--A comparison through simulations. Eng Fract Mech 2015;141:260–73.

[45] Tsuchiya M, Ueno H, Takagi I. Research of semi solid casting of iron. JSAE Rev 2003;24:205–14.

[46] mit Kugelgraphit G. Konstruiren+ Giessen. Zentrale für Gussvervendung 1988.

[47] Fundições T. Thermal conductivity of gray iron and compacted graphite iron used for cylinder heads. Rev Matéria 2005;10:265–72.

[48] Nagvendra Kumar kanoje, Satish C.Sharma, S.P.Harsha, EPFM analysis of subsurface crack beneath a wheel flat using dynamic condition, Procedia Materials science 6 (2014) 43-60.

[49] Singh KL, Keswani K, Vaggar M. Crack growth simulation of stiffened fuselage panels using XFEM techniques 2014.

APPENDIX

XFEM Modelling steps followed in ABAQUS

1. Module→Part

From the main menu bar, select Part→Create. Name the part 'WheelGeometry'. Modelling space is 3D, Type is Deformable, Base feature is 'Solid' and approximate size 200. Click continue.

To simplify/optimize the meshing process we create a series of partitions in the crack domain which separate the cracked region from the rest of the part.

Double click on the menu bar→Tools→Partition→ Face sketch→ Draw the middle section of the wheel representing the contact patch.

Partition→ cell→ Normal to edge to have three sections.

2. Module→Property

From the menu bar, select Material →Create. Name the material as **Grey cast iron**. And create the material property of the steel

i. General →Density
ii. Mechanical →Elasticity →Elastic: Under type choose Isotropic. Put the value of **Young's Modulus** and the **Poisson's ratio**.

Mechanical →Plasticity →Plastic: Under type choose Isotropic. And put the value of the value in Table 3-12 and Table 3-13.

Mechanical → Expansion (For the thermal load analysis): Under type choose Isotropic and Toggle on **Use temperature dependent data** with a reference temperature of 25^0C. Put the values in Table 3-14. iii. Thermal → Conductivity: Under type choose Isotropic. Toggle on use temperature dependent data as shown in Table 3-14.

iv. Thermal →Specific Heat: Under type choose Isotropic. Toggle on use temperature dependent data. Table 3-14.
v. Mechanical →Damage for Traction separation laws →Maxps Damage: Tolerance: 0.1. Put the maximum principal stress at room temperature (25 ^{o}C) and high temperature (500 ^{o}C) of **255 and 345 (N/mm^2)** respectively**.**

On the **Sub-options** select Damage Evolution menu section. Use Energy

type damage evolution for fracture energy at room temperature (25 ^{o}C) and high temperature (500 ^{o}C) of 11.71 and 50.76N/mm respectively. On the **sub-options** menu again select Damage stabilization cohesive as 0.08 for the viscosity coefficient (i.e. less than fracture energy fraction comparatively).

From the Main menu bar, select →Create →Name: 'Disc main' →category is solid, Type: Homogeneous→ Continue. In the Edit section dialogue box, under material pick

Grey cast iron. Select the Assign section icon and select the whole disc brake entire domain then toggle **Done**. In the edit section Assignment dialog box, select disc main, and Grey cast iron and click Ok.

3. Module →Mesh

Mesh →Element type→ Element library: Standard→ Type: 3D stress→Select full integration for the area of interest (or crack domain) and reduced integration for other areas and Element shape: Tet.

Mesh→ Mesh controls→ free **tet**.

Mesh→ Seeds→ Assign seeds by number as per Figure 3-13.

Part→ Assembly→ Instance→ Select disc and accept the default then Ok.

Creating XFEM Crack

1. **Module →Part**

   Double click on Parts. Enter name as 'crack', modelling space is 3D, Type is Deformable, Base feature is Shell, Type is Extrusion and Approximate size is 200 mm. Click **Continue**.

2. Expand 'Assembly', and then double click on instances. Select 'crack' and accept the default settings by clicking ok.
3. Select 'Interaction' from the main menu, click 'Special'. Name as: 'subsurface crack' Type is XFEM and continue. Select Interaction and Name it as 'Crack-XFEM' type is XFEM crack.

Create Boundary Conditions and Loads

1. From the main menu bar, select step →Create
2. Name it step-1. The Procedure type is General →Static, general.

3. In Edit step dialog box, under the basic tab, enter **Contact Pressure** as the description. Time period is 3.5 second.

And toggle on Incrementation: Type is Automatic. Maximum number of increments is **100000**. Increment size is from: **0.5** and minimum is **1E-20** and Maximum is **3.5**.

Select **other** and General solution controller →Edit →step-1 →continue →Toggle on Specify and Time increment →I_a from **5** to more than **20**. And toggle on Discontinuous analyses. Automatic damage stabilization specify dissipation energy fraction.

To Create the Boundary Condition

For the combined thermal and mechanical analysis:

Specify the maximum temperature rise at the disc brake surface by using material properties of disc brake at high temperature (500 ^{o}C).

From the main menu bar, select BC →Create: select step-1. Category is Mechanical. Type for selected step is Symmetry/Antisymmetric/Encastre. Name is Fixed End. Select the axial inserted place of hole and cutting surface to show the full model of disc simplified disc brake portion. Click Done and choose ENCASTRE from the Boundary dialogue box and click continue.

1. Double click on loads. Enter name as Contact Pressure, category is Mechanical, Type is Pressure, click continue. Magnitude is 0.251 (Mpa) and 0.254 (Mpa) at room temperature (25 ^{o}C) and high temperature (500 ^{o}C).

In order to visualize the crack in the output database the following changes need to be made to the step module:

Step module →Output →Field output requests→Manager→F-output-1→Edit → Expand Fracture/Failure →PHILSM (In order to see the crack) then State/Field/user/Time →STATUS XFEM (to see the status of the artificial crack, Propagating or static)-Put additional parameters like Von-mises stress and PEEQ (Equivalent plastic strain criterion) from Stress and strain menus.

MODULE→JOB

From the main menu bar, select Job→ Create. Enter any name for the job. Summit the job and monitor the progress. Then finally see the Results.